Journal of Medicinal Chemistry

Article

pubs.acs.org/jmc

Novel Second-Generation Di-2-Pyridylketone Thiosemicarbazones Show Synergism with Standard Chemotherapeutics and Demonstrate Potent Activity against Lung Cancer Xenografts after Oral and Intravenous Administration in Vivo

David B. Lovejoy,[†] Danae M. Sharp,[†] Nicole Seebacher,[†] Peyman Obeidy,[†] Thomas Prichard,[†] Christian Stefani,[†] Maram T. Basha,[‡] Philip C. Sharpe,[‡] Patric J. Jansson,[†] Danuta S. Kalinowski,[†] Paul V. Bernhardt,[‡] and Des R. Richardson*[,†]

[†]Iron Metabolism and Chelation Program, Department of Pathology and Bosch Institute, University of Sydney, Sydney, New South Wales 2006, Australia

[‡]School of Chemistry and Molecular Biosciences, University of Queensland, Brisbane, Queensland 4072, Australia

Supporting Information

ABSTRACT: We developed a series of second-generation di-2-pyridyl ketone thiosemicarbazone (DpT) and 2-benzoylpyridine thiosemicarbazone (BpT) ligands to improve the efficacy and safety profile of these potential antitumor agents. Two novel DpT analogues, Dp4e4mT and DpC, exhibited pronounced and selective activity against human lung cancer xenografts in vivo via the intravenous and oral routes. Importantly, these analogues did not induce the cardiotoxicity observed at high nonoptimal doses of the first-generation DpT analogue, Dp44mT. The Cu(II) complexes of these ligands exhibited potent antiproliferative activity having redox potentials in a range accessible to biological reductants. The activity of the copper complexes of Dp4e4mT and DpC against lung cancer cells was synergistic in combination with gemcitabine or cisplatin. It was demonstrated by EPR spectroscopy that dimeric copper compounds of the type $[CuLCl]_2$, identified crystallographically, dissociate in solution to give monomeric 1:1 Cu:ligand complexes. These monomers represent the biologically active form of the complex.

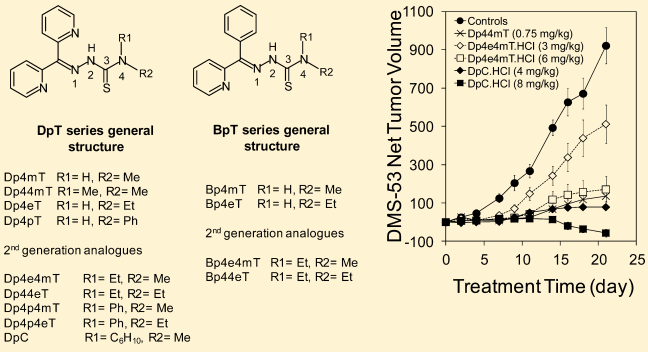

INTRODUCTION

Targeting the essential nutrient iron (Fe) is a promising approach for the treatment of cancer, reflecting the fact that neoplastic cells have higher Fe utilization due to their rapid replication relative to normal cells.[1,2] In fact, this increased use of iron is required for the activity of key Fe-containing proteins that catalyze critical reactions involved in energy metabolism, respiration, and DNA synthesis.[3−5] Consequently, due to this increased Fe requirement, neoplastic cells compared to their normal counterparts express higher levels of the transferrin receptor 1 that delivers iron from the Fe transport protein, transferrin (Tf).[1,2]

Considering the key role of Fe in tumor cell growth, the development of novel Fe-binding drugs (chelators) is a promising anticancer strategy,[1,5,6] as demonstrated by the entrance into clinical trials of the anticancer agent, 3-aminopyridine-2-carboxaldehyde thiosemicarbazone (3-AP). However, this chelator results in relatively low antitumor activity and its dose-limiting side effects such as methemoglobinemia and hypoxia have seriously limited its clinical potential.[7,8] Other classes of potential ligands that have shown marked antitumor activity are the di-2-pyridyl ketone thiosemicarbazones (DpT; Figure 1) and their 2-benzoylpyridine thiosemicarbazone (BpT; Figure 1) analogues.[9−12] Some of the DpT ligands overcome the disadvantages of 3-AP, in that they do not induce methemoglobinemia[13] and are markedly more active and selective.[10,14−16]

The most extensively evaluated DpT series analogue is di-2-pyridyl ketone 4,4,-dimethyl-3-thiosemicarbazone (Dp44mT; Figure 1), which demonstrated marked and selective activity against tumor xenografts in nude mice.[10,12] Significantly, Dp44mT was shown to mediate marked antitumor activity by Fe and copper (Cu) chelation and redox-cycling of the so-formed Fe and Cu complexes to generate reactive oxygen species (ROS).[12,17−19] Other modes of anticancer activity reported for Dp44mT and other chelators include up-regulation of the metastasis suppressor protein, N-myc downstream regulated gene-1 (NDRG1),[14,20−22] and modulation of the expression of the cyclin family of proteins (e.g.,

Received: June 3, 2012
Published: August 3, 2012

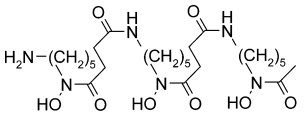

DFO

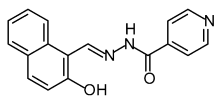

NIH

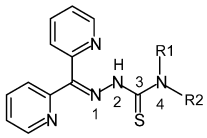

DpT series general structure

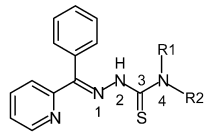

BpT series general structure

Dp4mT R1= H, R2= Me
Dp44mT R1= Me, R2= Me
Dp4eT R1= H, R2= Et
Dp4pT R1= H, R2= Ph

2nd generation analogues

Dp4e4mT R1= Et, R2= Me
Dp44eT R1= Et, R2= Et
Dp4p4mT R1= Ph, R2= Me
Dp4p4eT R1= Ph, R2= Et
DpC R1= C_6H_{10}, R2= Me

Bp4mT R1= H, R2= Me
Bp4eT R1= H, R2= Et

2nd generation analogues

Bp4e4mT R1= Et, R2= Me
Bp44eT R1= Et, R2= Et

Figure 1. Line drawings of the structures of the chelators, desferrioxamine (DFO), and 2-hydroxy-1-naphthaldehyde isonicotinoyl hydrazone (NIH; also known as 311) and the general structures of the DpT and BpT series of chelators. Substituents defining the first- and second-generation ligands are indicated.

cyclin D1), GADD family of proteins (e.g., GADD45), and cyclin-dependent kinase 2.[23,24] Significantly, the potent and selective antitumor activity of Dp44mT has been independently verified by others.[15,16,22] In particular, Rao and colleagues reported topoisomerase IIα inhibition and specific antitumor activity,[15] while Liu et al. demonstrated that Dp44mT markedly inhibits tumor cell metastasis in vivo through induction of NDRG1.[22] However, our laboratory reported that, at high nonoptimal doses, Dp44mT was found to induce cardiotoxicity in nude mice.[10] Hence, in an effort to develop highly potent, yet less toxic DpT chelators, we designed a second-generation of DpT ligands. These new agents were designed based upon a key structure–activity relationship derived from our previous studies[25] in which the replacement of the terminal H at N4 with an alkyl group increases antiproliferative activity.

The current investigation describes seven second-generation DpT and BpT analogues, and of these, two ligands, namely di-2-pyridyl ketone 4-ethyl-4-methyl-3-thiosemicarbazone (Dp4e4mT) and di-2-pyridyl ketone 4-cyclohexyl-4-methyl-3-thiosemicarbazone (DpC), were identified as having the best activity and safety profile in vivo. Major findings include that both agents exhibited marked activity in vivo against a human lung cancer xenograft after both intravenous and oral administration and that they did not induce cardiotoxicity, unlike the first-generation analogue, Dp44mT.[10] Indeed, the ability of these agents to be administered orally provides a significant pharmacological advantage for treatment relative to the more cumbersome intravenous route. Additionally, for the first time, we demonstrate that these agents and their copper complexes act synergistically with standard chemotherapeutics for lung cancer, namely gemcitabine and cisplatin.

RESULTS AND DISCUSSION

Chemistry Studies. *Ligand and Complex Synthesis and Characterization.* The second-generation thiosemicarbazone analogues were synthesized by standard methods involving a Schiff base condensation between the N^4-disubstituted thiosemicarbazide with di-2-pyridyl ketone or 2-benzoylpyridine, as reported for analogous compounds.[19,26] The ligands were not appreciably soluble in water at high concentrations but were highly soluble in polar aprotic solvents such as DMF, MeCN, and DMSO. The ^{1}H NMR spectral properties of the second-generation DpT and BpT ligands were very similar to those of the first-generation DpT and BpT chelators.[9,19]

The Cu^{II} and Fe^{III} complexes of thiosemicarbazones are known to possess potent antitumor activity and were synthesized according to previously published procedures.[19,27] Spectroscopic measurements (UV–vis and IR) confirmed the formation of each complex, and the properties mirrored those previously reported.[19,27] In DMF, the Cu^{II} complexes exhibited

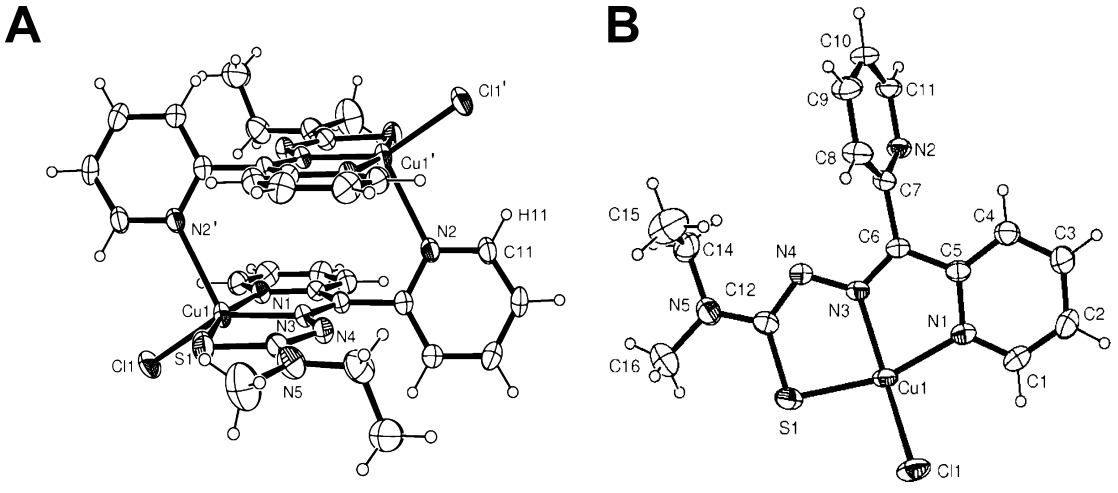

Figure 2. ORTEP views of: (A) the dimeric $[Cu(Dp4e4mT)Cl]_2$ complex and (B) the monomeric [Cu(Dp4e4mT)Cl] asymmetric unit. The 30% probability ellipsoids are shown. Selected bond lengths (Å) and angles (°): Cu1–N1 2.030(3), Cu–N3 1.987(3), Cu–S1 2.255(1), Cu–Cl1 2.285(1), Cu–N2′ 2.373(3), N1–Cu–S1 163.13(9), N3–Cu–Cl1 148.04(9), N1–Cu–N3 80.12(1), N3–Cu–S1 83.06(9), N2′–Cu-Cl1 94.88(7).

dx.doi.org/10.1021/jm300768u | J. Med. Chem. 2012, 55, 7230–7244

a weak visible absorption maximum (as a shoulder) in the region of 600 nm, which is most likely of d−d origin on the basis of their extinction coefficients and their energies which are as expected for a $Cu^{II}N_2SO$ or $Cu^{II}N_2SCl$ chromophore. The dominant peaks are due to ligand-centered transitions in the near UV. Overall, the electronic spectra of the Cu^{II} complexes mirror those of the related thiosemicarbazones such as [Cu(Dp44mT)(OAc)].[27] Similarly, the Fe^{III} complexes are spectroscopically indistinguishable from previously published pyridyl-thiosemicarbazone Fe^{III} complexes.[9,19,28]

Structural Characterization. The crystal structure of the Cu^{II} complex of Dp4e4mT (with chloride as the coligand) was determined considering the potent antitumor activity of this complex (see Biological Studies) and its likelihood to be involved in the biological activity of this thiosemicarbazone.[18] Although the expected tridentate N_2S coordination mode of the ligand was found, the structure is of a centrosymmetric, dimeric complex $[Cu(Dp4e4mT)Cl]_2$ where the distal pyridyl ring forms a bridge to an adjacent Cu^{II} ion (Figure 2A). The monomeric asymmetric unit comprising the equatorially coordinated $Dp4e4mT^-$ and Cl^- ligands is also shown (Figure 2B). The Cu(Dp4e4mT) moiety is essentially planar, with all three donor atoms and the metal lying within 0.03 Å of the least-squares plane defined by the CuN_2S array. The chlorido ligand is displaced by 1.16 Å from the CuN_2S plane to minimize repulsion of the *cis*-coordinated axial pyridyl ligand (C11−H11···Cl1′ 2.80 Å). The coordination sphere is completed by a weakly bound axial pyridyl ligand where the axial elongation is due to a Jahn−Teller distortion which markedly lowers the energy of the d_z2 orbital relative to the $d_x2_{-y}2$ orbital. The overall form of the five-coordinate geometry can be quantified by the τ parameter[29] which defines the degree of distortion between the extremes of square pyramidal ($\tau = 0$) and trigonal bipyramidal ($\tau = 1$) geometry on the basis of the coordinate angles [$\tau = (\alpha - \beta)60$, where α is the largest coordinate angle and β is the second largest coordinate angle]. For the structure of $[Cu(Dp4e4mT)Cl]_2$, a value of $\tau = 0.25$ was calculated, reflecting a distorted square pyramidal geometry.

Dimeric structures of this type have been seen in other Schiff base complexes comprising the di-2-pyridyl ketone moiety.[30,31] However, we have not structurally characterized any 1:1 Cu^{II} thiosemicarbazone complexes derived from chelators of the DpT class, and it appears likely that the self-assembly of Cu complex dimers, such as that seen in Figure 2A, is a characteristic feature of this group of ligands.

Because of the ability of these compounds to act as potent Fe chelators in cells in culture (see Biological Studies), the structure of the Fe^{III} complex $[Fe(DpC)_2]ClO_4$ was also examined. There were no unusual features of this complex which is similar to other low spin Fe^{III} thiosemicarbazone complexes reported by our laboratory.[28] The anionic ligands coordinate to Fe in a tridentate manner, typical for chelators from the BpT and DpT series, in their imine-thiolate resonance forms as NNS donors.[9,19] The three donor atoms are in a *syn* disposition as found previously for other members of this family.[9,19] These data above demonstrating complexation of Fe and Cu are significant, as the biological activity of this class of ligands is mediated through the binding of both these intracellular metals with the subsequent formation of cytotoxic redox-active complexes.[12,18,19] Indeed, we show below that Cu complexation leads to potent antitumor efficacy and it is likely that because cells contain both Fe and Cu, complexes of both types will form and mediate biological activity, as shown for the closely related DpT analogue, Dp44mT.[18]

Solution Structure. The dimeric solid state structure of $[Cu(Dp4e4mT)Cl]_2$ (Figure 2A) certainly does not persist in solution. In fact, EPR spectra of [Cu(Dp4e4mT)(OAc)], [Cu(Dp4e4mT)Cl], [Cu(DpC)(OAc)], and [Cu(DpC)Cl] were measured in frozen DMF solution (Figure 3), with each

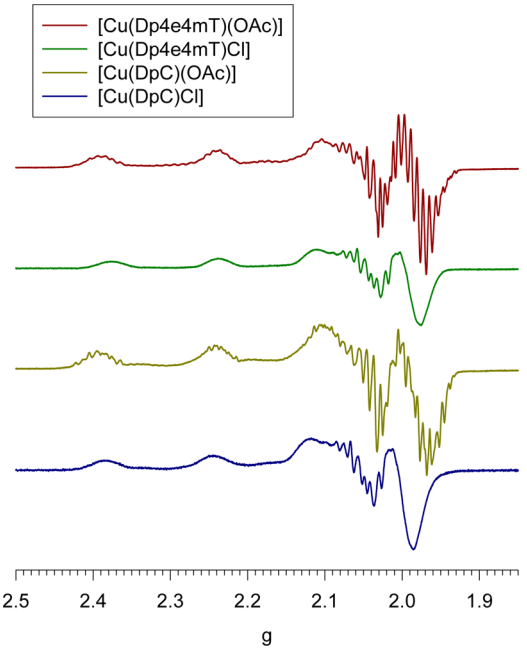

Figure 3. X-band EPR spectra of [Cu(Dp4e4mT)(OAc)], [Cu-(Dp4e4mT)Cl], [Cu(DpC)(OAc)], and[Cu(DpC)Cl] (1 mM) in frozen DMF solution (140 K).

spectrum being consistent with a monomeric Cu^{II} complex in a tetragonally elongated square pyramidal coordination environment ($g_z \gg g_{x,y}$, $A_z \gg A_{x,y}$).[32] No evidence for dimer formation through dipole−dipole coupling in the EPR spectrum was apparent, thus complete dissociation into monomeric 1:1 Cu:ligand complexes occurs in a solution of DMF and water (see below). The EPR spectra were simulated (see Supporting Information Figures S1−S4) in order to obtain accurate spin Hamiltonian parameters. Partial chlorido ligand dissociation of [Cu(Dp4e4mT)Cl] and [Cu(DpC)Cl] in DMF solution was suppressed by the addition of an excess of Et_4NCl. In contrast, the acetato complexes were more stable and no evidence of dissociation was found. In addition to hyperfine coupling with the Cu nucleus (^{63}Cu, ^{65}Cu: $I = 3/2$), which generates three sets of four lines centered at g_z, g_y, and g_x, ligand-centered superhyperfine coupling was superposed in the spectra of the OAc^- complexes. The two *cis* coordinated *N*-donors in the *xy* plane bear a nuclear spin of $I = 1$ and split each peak into a quintet. Long range superhyperfine coupling, probably from the noncoordinated N4 (Cu···N4 2.96 Å), may be responsible for the added fine structure, but this was not modeled in the simulation. This superhyperfine coupling was completely absent in the spectra of the two chlorido complexes, [Cu(Dp4e4mT)Cl] and [Cu(DpC)Cl], due presumably to broadening from unresolved superhypefine coupling with the chlorido ligands (^{35}Cl, ^{37}Cl: $I = 3/2$).

In each case, the EPR spectra in Figure 3 mimic those of the previously reported monomeric [Cu(Dp44mT)(OAc)] com-

dx.doi.org/10.1021/jm300768u | J. Med. Chem. 2012, 55, 7230−7244

plex[27] and unequivocally show that the solid state structure is not representative of its solution structure. In previous studies, we isolated six-coordinate 1:2 Cu:ligand complexes of related thiosemicarbazones[27] but found that partial dissociation was spontaneous, leading to the corresponding 1:1 Cu:ligand complex in solution.

Electrochemistry. Cyclic voltammetry of the Cu complexes in mixed DMF:H_2O (2:1) was carried out (Figure 4) to determine the $Cu^{II/I}$ redox potentials and to assess whether the complexes might be able to mediate Cu-catalyzed Fenton chemistry. This solvent combination was used to obtain sufficiently high concentrations of the copper complexes in solution. Under these conditions, the four complexes gave almost identical voltammograms with quasireversible $Cu^{II/I}$ couples at −90 mV versus the non-hydrogen electrode (NHE; Figure 4). This suggests that the Cl^- and OAc^- ligands are replaced by water in mixed DMF:water. This was confirmed by equivalent voltammetry experiments conducted in 100% DMF, where significantly different voltammograms were obtained for the acetato and chlorido complexes (see Supporting Information Figure S5). Partial dissociation of the chlorido complexes (in this case with no additional chloride ions present) was evident to give the DMF-coordinated analogues from the presence of a dominant high potential wave from $[Cu(DpC)(DMF)]^{+/0}$ and $[Cu(Dp4e4mT)(DMF)]^{+/0}$ (Supporting Information Figure S5) and a minor low potential wave from the corresponding chlorido complexes. Very similar behavior has been reported for related dithiocarbazate Schiff base complexes of Cu(II).[33] In either solvent (DMF or water/DMF), the voltammograms were insensitive to the change from ethyl (Dp4e4mT) to cyclohexyl (DpC). The reversible electrochemical behavior of these Cu complexes observed at a relatively high potential suggests that the Cu(II) complexes can easily be reduced in vivo and participate in redox cycling and ROS generation. This may be a factor in their potent antiproliferative activity (see Biological Studies).

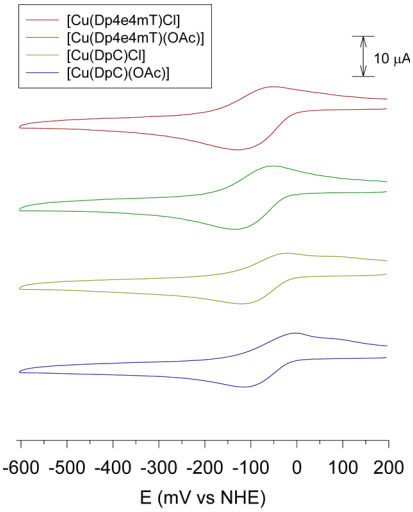

Figure 4. Cyclic voltammograms of [Cu(Dp4e4mT)Cl], [Cu(Dp4e4mT)(OAc)], [Cu(DpC)Cl], and [Cu(DpC)(OAc)] (1 mM in DMF:H_2O 2:1) at a sweep rate of 100 mV s^{-1}.

Biological Studies. *Novel Second-Generation DpT and BpT Analogues Exhibit Potent Antiproliferative Activity against SK-N-MC Neuroepithelioma Cells.* The second-generation DpT and BpT chelators were designed by specific replacement of the H atom at the terminal N4 atom (Figure 1) with alkyl and aryl groups in order to increase their lipophilicity and potentially enhance antitumor activity.[25] In these experiments, the first-generation chelators still bearing the terminal H atom were directly compared to the novel second-generation analogues in terms of their antiproliferative activity in vitro. For these studies, we initially utilized the SK-N-MC cell line as its response to chelators has been extensively examined in our laboratory.[25,34,35] Additionally, the positive control chelators, namely desferrioxamine (DFO), 2-hydroxy-1-naphthaldehyde isonicotinoyl hydrazone (NIH; also known as 311), and Dp44mT, were also assessed as their antiproliferative activity has been well characterized in this cell line.[25,34,35]

In good agreement with previous studies,[12,19] DFO and NIH exhibited moderate antiproliferative activity against SK-N-MC cells, with NIH being more active than DFO (Table 1). The concentrations of DFO and NIH required to inhibit cell growth to 50% of the untreated control (IC_{50}) were 10 ± 1 and 1.1 ± 0.3 μM, respectively (Table 1). However, Dp44mT potently inhibited proliferation of SK-N-MC cells (IC_{50}: 0.004 ± 0.002 μM), being far more active than DFO or NIH, as shown previously.[12,19] The new second-generation compounds also all exhibited significantly ($p < 0.001$) greater antiproliferative activity than DFO or NIH against SK-N-MC cells (Table 1). The analogues Dp4e4mT, Dp44eT, and Dp4p4mT were the most effective second-generation DpT series chelators, having IC_{50} values (0.004−0.006 μM) that were similar to Dp44mT (Table 1).

Table 1. Antiproliferative Activity (IC_{50}) of the First-Generation DpT and BpT Chelators Compared to the Second-Generation Analogues and the Positive Control Chelators, DFO, NIH and Dp44mT, as Determined Using SK-N-MC Cells after a 72 h Incubation[a]

chelator	IC_{50} (μM) SK-N-MC
DFO	10 ± 1
NIH	1.1 ± 0.3
Dp44mT	0.004 ± 0.002
first-generation analogues	
Dp4mT	0.3 ± 0.1
Dp4eT	0.06 ± 0.01
Dp4pT	0.02 ± 0.01
Bp4mT	0.018 ± 0.004
Bp4eT	0.012 ± 0.002
second-generation analogues	
Dp4e4mT	0.004 ± 0.002
Dp44eT	0.005 ± 0.002
Dp4p4mT	0.006 ± 0.001
Dp4p4eT	0.010 ± 0.002
DpC	0.013 ± 0.002
Bp4e4mT	0.006 ± 0.001
Bp44eT	0.011 ± 0.003

[a]Results are mean ± SD (three experiments).

A significant ($p < 0.001$) increase in antiproliferative activity was apparent when examining the least active first-generation ligand, Dp4mT (IC_{50}: 0.3 ± 0.1 μM; Table 1), with the least active second-generation analogue, DpC (IC_{50}: 0.013 ± 0.002 μM; Table 1), which showed 23-fold greater activity. This demonstrated the success of our ligand design strategy (Table 1

dx.doi.org/10.1021/jm300768u | J. Med. Chem. 2012, 55, 7230−7244

and Figure 5A) and could be due to their increased lipophilicity and membrane permeability. The first-generation BpT chelators, Bp4mT and Bp4eT, showed antiproliferative activity against SK-N-MC cells that was also markedly more potent than DFO or NIH in accordance with previous studies.[9] The second-generation Bp4e4mT and Bp44eT chelators demonstrated similar or greater antiproliferative efficacy than the corresponding parent BpT first-generation chelators (Table 1).

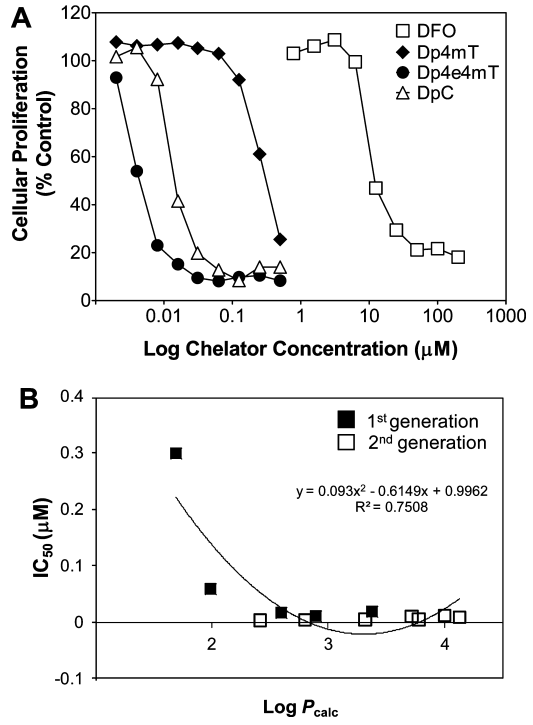

Figure 5. (A) A marked increase in antiproliferative activity is apparent for the second-generation analogues (Dp4e4mT and DpC) relative to their first-generation counterpart (Dp4mT) due to the replacement of the N4-terminal H with alkyl or aryl substituents. These studies demonstrate the success of the design strategy implemented in the current investigation. Results are from MTT proliferation assays examining the effects of the ligands on the growth of SK-N-MC cells over a 72 h incubation. Results are means of three experiments. (B) Relationship between the antiproliferative activity (IC_{50}) and lipophilicity (log P_{calc}) of the chelators using SK-N-MC neuroepithelioma cells. The IC_{50} (measured after a 72 h incubation) and log P_{calc} values for the second-generation DpT and BpT analogues and their parent compounds (Dp4mT, Dp4eT, Dp4pT, Bp4mT, and Bp4eT) were plotted. Lines were fitted in (A) and (B) using Microsoft Excel 2007 (Microsoft, Redmond, WA).

To assess the optimal octanol:water partition coefficient required for potent antiproliferative activity in SK-N-MC cells, the log P_{calc} values of the first- and second-generation DpT and BpT analogues were plotted against their IC_{50} values (Figure 5B). This demonstrated that an optimal lipophilic range existed, with ligands having log P_{calc} values between ~2.5 and 4.0, demonstrating the greatest antiproliferative efficacy. Significantly, optimal activity was observed at a log P_{calc} value of ~3.2 (Figure 5B). Importantly, more hydrophilic compounds of this class with log P_{calc} values lower than 2.5 may have difficulty crossing the cell membrane, while more lipophilic thiosemicarbazones with log P_{calc} values greater than 4.0 may become trapped in the lipid membrane. Significantly, the log P_{calc} values of the majority of the second-generation DpT and BpT chelators were found to lie within this optimal lipophilic range (Figure 5B). The optimal lipophilicity of the second-generation DpT and BpT chelators may be a critical factor in their increased antiproliferative activity in comparison to their parent first-generation analogues, which were generally less lipophilic (Figure 5B). We have recently observed a similar relationship with a related class of thiosemicarbazones,[36] and this demonstrates the important correlation between optimal lipophilicity and potent antiproliferative activity of thiosemicarbazone chelators.

Novel Second-Generation DpT and BpT Analogues Inhibit Cellular ^{59}Fe Uptake from ^{59}Fe Transferrin and Mediate Efflux of ^{59}Fe from Cells. Our previous studies have related chelator antiproliferative activity to the prevention of cellular Fe uptake and to the ability to increase Fe mobilization from cells.[35,36] Hence, the efficacy of the second-generation DpT and BpT chelators to inhibit ^{59}Fe uptake from the serum Fe-binding protein, Tf, in SK-N-MC neuroepithelioma cells was assessed and compared to first-generation chelators. Again, these cells were used as their response to chelators in Fe uptake and efflux studies has been well characterized in our laboratory.[25,34,35] The positive control ligands, NIH and Dp44mT, were very effective in limiting cellular ^{59}Fe uptake to 5.3 ± 1.2% and 3.5 ± 1.4% of the control, respectively (Figure 6A), and were far more active than the hydrophilic chelator, DFO, that only limited ^{59}Fe uptake to 84 ± 5% of the control (Figure 6A). These results were in good agreement with our previous studies.[9,25] Generally, the majority of the second-generation DpT and BpT chelators were slightly less effective than their first-generation counterparts (Figure 6A). For instance, while Dp4e4mT showed 75-fold greater antiproliferative efficacy than its first-generation parent, Dp4mT, in terms of preventing ^{59}Fe uptake, Dp4e4mT was almost half as effective as Dp4mT (12.3% cf. 6.9% of the control; Figure 6A). The only exception was the second-generation chelator, Dp44eT, which was approximately twice as effective at inhibiting ^{59}Fe uptake as the relative first-generation ligand, Dp4eT. However, all second-generation compounds showed markedly and significantly ($p < 0.001$) greater activity than DFO (Figure 6A).

Assessing the ability of these ligands to mobilize ^{59}Fe from SK-N-MC cells, and in agreement with previous investigations,[9,12] the positive control chelators, DFO, NIH, and Dp44mT, were able to release 15.2 ± 0.9%, 44.9 ± 1.5%, and 45.0 ± 3.0% cellular ^{59}Fe, respectively, while control medium alone only led to the release of 6.4 ± 0.7% of ^{59}Fe (Figure 6B). While all the second-generation chelators were more active than DFO at mobilizing cellular ^{59}Fe, they were generally less active than the corresponding first-generation analogues. The most effective second-generation chelators at mobilizing cellular ^{59}Fe were Dp4e4mT, Dp44eT, and Dp4p4mT, which had comparable efficacy as their first-generation counterparts (Figure 6B). However, notably lower activity at inducing ^{59}Fe efflux was identified for the second-generation chelators, Dp4p4eT, DpC, Bp4e4mT, and Bp44eT, relative to the first-generation analogues (Figure 6B).

An optimal log P_{calc} value was demonstrated by examining the relationship between the log P_{calc} values of the first- and second-generation analogues and their ability to inhibit ^{59}Fe uptake (Figure 6C) or mobilize cellular ^{59}Fe (Figure 6D). In fact, analogues with a log P_{calc} value of 2−2.5 were able to effectively inhibit ^{59}Fe uptake and mobilize cellular ^{59}Fe, while the second-generation chelators that generally had higher log P_{calc} values were less efficient (Figures 6C,D). This may reflect

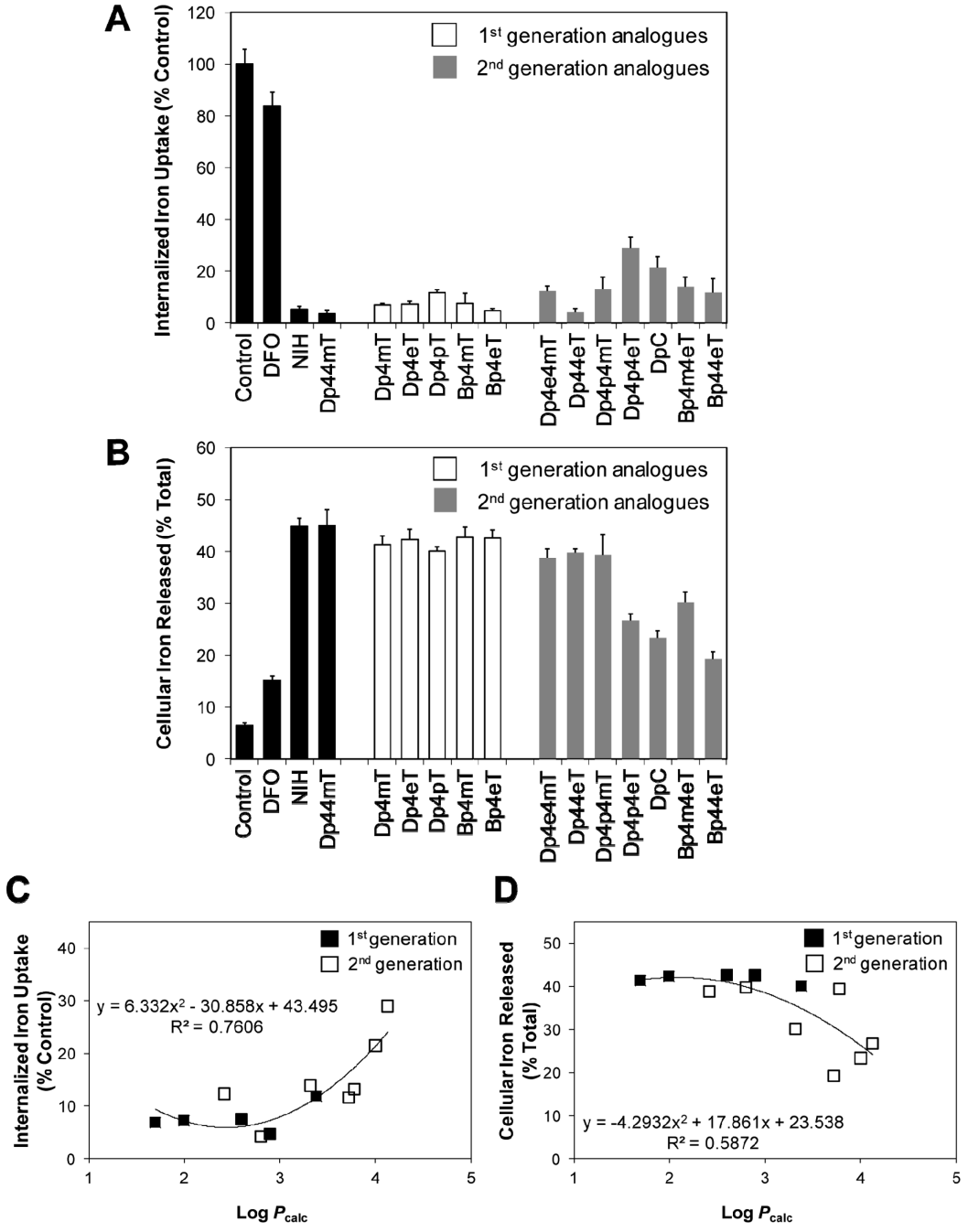

Figure 6. The effect of the first-generation analogues relative to their second-generation counterparts on: (A) inhibition of internalized ^{59}Fe uptake from ^{59}Fe-transferrin (Tf) by SK-N-MC cells and (B) promotion of cellular ^{59}Fe release from prelabeled SK-N-MC cells. The relationships between (C) the inhibition of internalized ^{59}Fe uptake from ^{59}Fe-Tf and (D) the cellular ^{59}Fe release against lipophilicity (log P_{calc}) of the second-generation DpT and BpT analogues and their parent compounds (Dp4mT, Dp4eT, Dp4pT, Bp4mT, and Bp4eT) using SK-N-MC neuroepithelioma cells were plotted. (A) Cells were labeled with ^{59}Fe-Tf (0.75 μM) for 3 h/37 °C in the presence or absence of chelators (25 μM) and then washed four times on ice with ice-cold PBS. Internalized ^{59}Fe uptake was determined using Pronase (1 mg/mL). (B) Cells were prelabeled with ^{59}Fe-Tf (0.75 μM) for 3 h/37 °C and then washed fpir times on ice with ice-cold PBS. The cells were then reincubated in the presence or absence of chelators (25 μM) for 3 h/37 °C and ^{59}Fe release examined. The results in (C) and (D) are plotted against log P_{calc}, which was calculated using ChemDraw v4.5 (CambridgeSoft, Cambridge, MA) and lines fitted using Microsoft Excel 2007. Results are mean ± SD (three experiments).

the optimal log *P* value necessary for the resultant hydrophobic iron complex to pass through cellular membranes and efficiently mobilize iron from cells. In fact, the most lipophilic second-generation analogues may form highly hydrophobic iron complexes that become trapped within cellular membranes, preventing iron mobilization.

Because the majority of the second-generation ligands showed greater antiproliferative efficacy than first-generation analogues, despite showing less Fe chelation activity, suggests their antitumor effect does not solely depend on cellular Fe complexation. Indeed, we showed that chelators of this class form highly redox active Fe and Cu complexes that generate cytotoxic ROS.[12,18,19] Additionally, DpT and BpT class

dx.doi.org/10.1021/jm300768u | J. Med. Chem. 2012, 55, 7230−7244

chelators were also demonstrated to have multiple molecular targets including ribonucleotide reductase,[3] thiol-containing systems,[37] molecules involved in cell cycle control e.g., cyclin D1,[23,38] and the metastasis suppressor, NDRG-1.[14,20,22]

Activity of the Second-Generation Analogues Against Lung Cancer In Vitro and In Vivo: Identification of Dp4e4mT and DpC as Potent Anti-Tumor Agents. Considering the marked antiproliferative activity of the second-generation analogues (Table 1) and also the impressive efficacy of the first-generation analogues against lung cancer cells and a lung tumor xenograft,[10,11] we then investigated the activity of the second-generation series against this tumor type. Preliminary investigations in vivo of all second-generation analogues demonstrated that Dp4e4mT and DpC were the most effective against this tumor (data not shown). Moreover, these analogues were novel compounds which enabled patent protection[39] and potential further development as pharmaceuticals. Hence, the studies reported below in vitro and in vivo focus on these two highly active agents.

Dp4e4mT and DpC Exhibit Marked Antiproliferative Activity Against Lung Cancer Cells in Vitro and Act Synergistically with Currently Used Chemotherapeutics. The antiproliferative activity of Dp4e4mT and DpC was examined using DMS-53 small cell lung cancer cells and A549 non-small cell lung carcinoma cells in vitro over a 72 h incubation (Table 2). Both Dp4e4mT and DpC potently inhibited DMS-53 and A549 cell proliferation, generally showing slightly more activity than the first-generation chelator, Dp44mT (Table 2). For example, against A549 cells, DpC was 5-fold more active than Dp44mT. Significantly, Dp4e4mT and DpC were also at least 137-fold more active than DFO or NIH (Table 2). Importantly, in comparison to the standard chemotherapeutics, cisplatin and etoposide, that are used for lung cancer treatment,[40−42] Dp4e4mT and DpC exhibited pronounced and significantly ($p < 0.001$) greater activity against DMS-53 and A549 cells (Table 2). Additionally, these second-generation chelators exhibited comparable or better activity than the chemotherapeutic, gemcitabine,[40−42] again confirming their promise as anticancer agents.

Table 2. Antiproliferative Activity (IC_{50}) of Dp4e4mT and DpC and their HCl Salts Compared to the the Positive Control Chelators DFO, NIH and Dp44mT and the Chemotherapeutics, Gemcitabine, Cisplatin, and Etoposide as Determined Using DMS-53 and A549 Lung Carcinoma Cells after a 72 h incubation[a]

	IC_{50} (μM)		
agents	DMS-53	A549	MRC-5
DFO	10 ± 1	7.5 ± 0.6	>10
NIH	1.1 ± 0.3	2.2 ± 0.2	>10
Dp44mT	0.010 ± 0.002	0.020 ± 0.008	>10
Dp4e4mT	0.008 ± 0.002	0.010 ± 0.004	>10
Dp4e4mT·HCl	0.006 ± 0.001	0.001 ± 0.004	>10
DpC	0.008 ± 0.004	0.004 ± 0.001	>10
DpC·HCl	0.007 ± 0.004	0.004 ± 0.001	>10
gemcitabine	0.009 ± 0.003	0.02 ± 0.01	
cisplatin	2.2 ± 0.8	8 ± 3	
etoposide	1.5 ± 0.6	0.8 ± 0.3	

[a]The antiproliferative activity of these agents is far less in mortal MRC-5 fibroblasts relative to the lung cancer cells. Results are mean ± SD (three experiments).

To improve the solubility of these second-generation chelators for oral in vivo tumor studies (see below), hydrochloride salts of the agents were prepared. Comparing their antiproliferative activity, the hydrochloride salts of Dp4e4mT and DpC showed similar antiproliferative activity to their base forms (Table 2). Another important pharmacological aspect of chemotherapy is the ability to target tumor cells while leaving normal cells unaffected. Hence, we next examined the effect of the chelators on the growth of mortal MRC-5 fibroblasts (Table 2). Significantly, these cells were at least a 1000-fold more resistant to the effects of the second-generation ligands compared to lung cancer cells, suggesting the existence of an exploitable "chemotherapeutic window" of selectivity.

Current chemotherapy for cancer often uses combinations of two or more drugs.[40−42] This approach offers enhanced synergistic therapeutic efficacy, improved selectivity, lower toxicity, and helps overcome drug resistance.[43] The chemotherapy of small cell lung carcinoma often consists of a platinum drug in combination with etoposide, whereas a combination of cisplatin and gemcitabine is frequently used for treatment of nonsmall cell lung carcinoma.[40−42] Considering this, we then examined if DpC·HCl or Dp4e4mT·HCl work synergistically with standard chemotherapy regimens for lung cancer (Figure 7A). To potentially provide mechanistic insights, we included in these experiments DFO and Dp44mT as relative controls and the Cu(II) complexes of

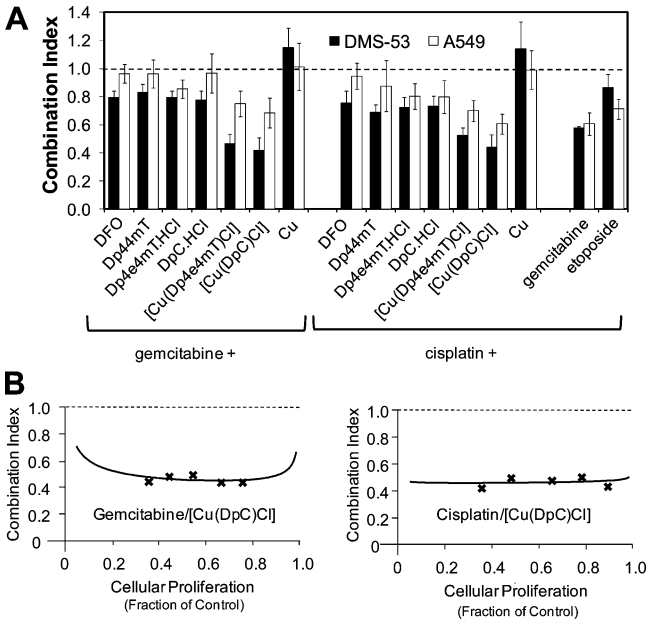

Figure 7. Demonstration of synergy of DpC, Dp4e4mT, or their copper complexes when combined with either gemcitabine or cisplatin. (A) Combination index (CI) plot of DpC, Dp4e4mT, or their copper complexes when combined with either gemcitabine or cisplatin after a 72 h incubation with either DMS-53 or A549 lung cancer cells. These results are compared with the controls, DFO, Dp44mT, $CuCl_2$, gemcitabine, or etoposide when combined with gemcitabine or cisplatin. (B) Fractional affect−combination index plot for the combination of gemcitabine and the DpC copper complex ([Cu(DpC)Cl]) or cisplatin and [Cu(DpC)Cl] using DMS-53 cells and a 72 h incubation with these agents. Plots were calculated according to the Chou−Talalay method[44−46] using CalcuSyn software (Biosoft, Cambridge, UK). Results are mean ± SD (three experiments).

dx.doi.org/10.1021/jm300768u | J. Med. Chem. 2012, 55, 7230−7244

DpC or Dp4e4mT that can probably form intracellularly. The latter complexes were also assessed by considering that the Cu(II) complexes of related DpT ligands show marked antitumor activity due to their ability to redox cycle and generate cytotoxic ROS.[18] In these studies, we used the method of Chou−Talalay,[44,45] which provides a rigorous assessment of drug−drug interactions based on drug−response curves to generate a combination index (CI) that quantifies synergistic activity.[44,46] In fact, CI values of <1, 1, and >1 indicate synergistic, additive, and antagonistic effects, respectively.[44,46] Interestingly, DFO exhibited moderate synergism with gemcitabine or cisplatin against DMS-53 cells, as defined by the CI values of 0.80 ± 0.04 and 0.75 ± 0.08, respectively (Figure 7A). However, against A549 cells, DFO interactions with gemcitabine or cisplatin and were nearly additive (Figure 7A). The first-generation chelator Dp44mT showed similar results to DFO against DMS-53 cells. In addition, this chelator showed a slightly greater synergistic effect in combination with cisplatin than with gemcitabine in DMS-53 cells (Figure 7A). Moderate synergism was also evident for Dp4e4mT·HCl or DpC·HCl in combination with gemcitabine or cisplatin against DMS-53 cells. However, only Dp4e4mT·HCl retained synergism against A549 cells in the presence of gemcitabine (Figure 7A).

Surprisingly, the copper complexes of both DpT analogues (i.e., [Cu(Dp4e4mT)Cl] and [Cu(DpC)Cl]) were markedly and significantly ($p < 0.001$) more synergistic than the free ligands in combination with gemcitabine or cisplatin against DMS-53 and A549 cells. Specifically, [Cu(DpC)Cl] in combination with gemcitabine or cisplatin against DMS-53 cells resulted in CI values of 0.42 ± 0.09 and 0.44 ± 0.09, respectively (Figure 7A). To ensure that these results were due to the formation of copper thiosemicarbazone complexes, we included $CuCl_2$ alone as a relative control. In clear contrast, these results showed that copper ions were nearly additive or produced mildly antagonistic effects in combination with gemcitabine or cisplatin against both cell types (Figure 7A). As it is possible that the nature of drug−drug interactions can change as a function of concentration or activity, we generated a fractional affect−combination index plot to assess the synergism between [Cu(DpC)Cl] and gemcitabine or cisplatin.[44,46] These data show that the interaction of [Cu(DpC)Cl] with both these chemotherapeutics is synergistic over a range of activity levels (Figure 7B).

Considering these results in Figure 7, it is conceivable that the chelation of cellular copper may be important in terms of the mechanism of synergism observed with the ligands and the chemotherapeutics. Importantly, the synergism exhibited by the second-generation chelators and their copper complexes was generally comparable to standard drug therapy regimens. In particular, DFO, Dp44mT, Dp4e4mT·HCl, and DpC·HCl were all more synergistic against DMS-53 cells than the combination of etoposide and cisplatin that is the foundation of chemotherapy regimens for small cell lung carcinoma.[41,42] Against A549 cells, [Cu(Dp4e4mT)Cl] and [Cu(DpC)Cl] exhibited comparable synergism to the standard chemotherapy regimen of gemcitabine and cisplatin. Collectively, Dp4e4mT·HCl and DpC·HCl have synergistic potential in combination with standard chemotherapy regimens for lung cancer.

Dp4e4mT and DpC Exhibit Potent and Selective In Vivo Antitumor Activity Against Lung Cancer Xenografts in Mice by both the Intravenous and Oral Routes. The marked activity of Dp4e4mT and DpC observed in vitro indicated that studies in vivo against DMS-53 tumor xenografts in nude mice were important to perform to assess efficacy. This tumor was used to provide a relevant comparison to our investigations using Dp44mT and other ligands.[10,11] Initial studies examined chelator efficacy when given by iv administration, as our previous studies demonstrated that this route of administration showed good tolerability with potent antitumor activity.[10] When DMS-53 xenografts had reached 100 mm^3 in volume, treatment began with either the vehicle control, the positive control chelator, Dp44mT, which was given as the base form in accordance with our previous studies (0.75 mg/kg iv; 5 days/week),[10] Dp4e4mT·HCl (3 or 6 mg/kg iv; 5 days/week), or DpC·HCl (4 or 8 mg/kg iv; 5 days/week). The 0.75 mg/kg dose of Dp44mT was used considering our in vivo studies where it led to marked inhibition of tumor growth.[10] The doses selected for DpC·HCl and Dp4e4mT·HCl represented the maximum tolerated (MTD) and half-MTD doses (data not shown).

After 21 days of treatment, tumors in nude mice receiving the vehicle control grew rapidly, reaching an average net volume of 922 ± 94 mm^3 (Figure 8A). Importantly, Dp44mT, Dp4e4mT·HCl, and DpC·HCl all significantly ($p < 0.01$−0.001) reduced the net growth of DMS-53 tumor xenografts relative to the control after the 21 day treatment schedule (Figure 8A). However, the most effective agent was DpC·HCl (8 mg/kg), which markedly and significantly ($p < 0.001$) decreased tumor volume versus the control (Figure 8A). In fact, tumor volume began to decrease in size relative to day 0 (untreated mice) after 16 days of treatment with DpC·HCl (8 mg/kg; Figure 8A). At a lower dose of 4 mg/kg, DpC·HCl also significantly ($p < 0.001$) limited tumor volume to 79 ± 14 mm^3 relative to the vehicle control (922 ± 94 mm^3) after 21 days of treatment. Notably, DpC·HCl (4 or 8 mg/kg) was significantly ($p < 0.001$) more effective and less toxic (see Toxicology) than the first-generation chelator, Dp44mT (0.75 mg/kg), that significantly ($p < 0.001$) reduced net tumor volume to 136 ± 28 mm^3 after 21 days of treatment relative to the vehicle control (Figure 8A). Notably, Dp4e4mT·HCl (3 and 6 mg/kg) also significantly ($p < 0.001$−0.05) reduced net tumor volume to 512 ± 101 mm^3 and 171 ± 67 mm^3, respectively, after 21 days treatment when compared to the vehicle-treated control mice (Figure 8A). At 6 mg/kg, Dp4e4mT·HCl did not show any significant difference in activity to Dp44mT (0.75 mg/kg; Figure 8A). However, importantly, Dp4e4mT·HCl showed less toxicity (see Toxicology). The length of treatment used in this experiment was limited by tumor size in the vehicle control group. As tumor size approached the maximum limit (1000 mm^3) prescribed by the local animal ethics committee by day 21, it was not possible to continue the experiment. After 21 days of treatment, the mice were sacrificed and tumors were excised and weighed. Control tumors weighed 0.83 ± 0.11 g, whereas mice receiving 4 or 8 mg/kg of DpC·HCl led to significantly ($p < 0.001$) smaller tumors that weighed 0.15 ± 0.02 g and 0.06 ± 0.02 g, respectively (Figure 8B). Tumors from mice given Dp44mT (0.75 mg/kg) weighed 0.27 ± 0.04 g, a result that was comparable to tumors excised from Dp4e4mT·HCl (6 mg/kg)-treated mice which weighed 0.40 ± 0.10 g (Figure 8B). Hence, DpC·HCl was significantly ($p < 0.05$) more effective than Dp44mT at reducing tumor weight. Importantly, all tumor weights were consistent with measured tumor volumes.

Toxicology Following iv Administration. Body and Organ Weights. Measurement of these indices provided an initial

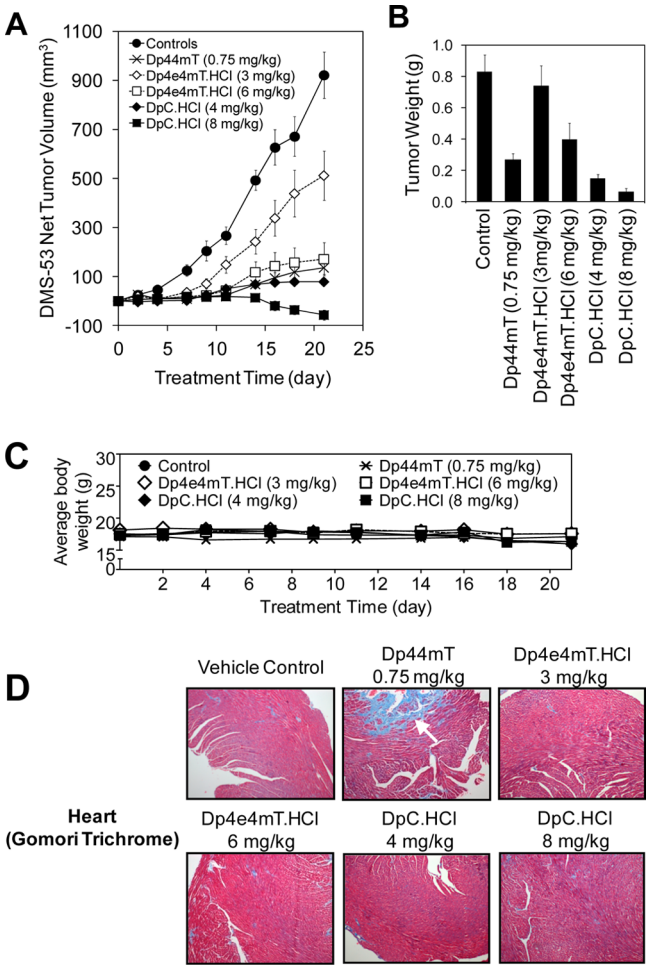

Figure 8. DpC and Dp4e4mT demonstrate marked antitumor activity against human DMS-53 lung tumor xenografts in nude mice after intravenous (iv) administration and do not induce cardiotoxicity. (A) Net tumor volume as a function of time of DMS-53 xenografts after iv administration (tail vein) of vehicle control (30% propylene glycol/saline), Dp44mT (0.75 mg/kg), Dp4e4mT·HCl (3 or 6 mg/kg), or DpC·HCl (4 or 8 mg/kg). (B) Tumor weights (wet weight) from the study in (A) after sacrifice of the animals on day 21. (C) Average body weights of nude mice for the study in (A) during treatment with the agents for 21 days. (D) Histological sections of the hearts taken from the mice in (A) after 21 days of treatment and stained with Gomori Trichrome to detect fibrosis (see arrow; magnification 100×). Results in (A–C) are mean ± SD (n = 6–7 mice/condition), while the photographs in (D) are typical of the histology observed.

assessment of toxicity following euthanasia. In all treatment groups, body weight did not significantly change from the pretreatment measurement (Figure 8C), indicating that the chelators did not affect appetite or otherwise induce cachexia. Preliminary studies defined the MTD over a 42 day period, and some moderate weight loss was expected. However, due to the early termination after 21 days due to rapid tumor growth in vehicle-treated mice, no weight loss was found. Additionally, no significant differences were found in any organ weights between the different treatment groups, apart from significant (p < 0.05–0.01) increases in liver weight in Dp4e4mT·HCl (3 and 6 mg/kg) and DpC·HCl (8 mg/kg) treated mice relative to the vehicle control (Supporting Information Table S1).

Hematological Indices. To further explore whether chelator treatment induced other toxic effects, we examined a panel of hematological indices. As Fe chelating agents have the potential to induce iron deficiency, it was vital to carefully assess these parameters. Importantly, no significant difference was found in the red blood cell (RBC) count between the vehicle-treated control and most treatment groups (Supporting Information Table S2). This was probably due to the low doses of ligands utilized. However, in mice treated with DpC·HCl (8 mg/kg), a significant (p < 0.05–0.01) decrease in RBC count and hemoglobin level in addition to a significant (p < 0.01) increase in reticulocyte count and % reticulocytes was found, indicating a mild anemia. The higher dose of Dp4e4mT·HCl (6 mg/kg) also resulted in a significant (p < 0.01) increase in reticulocyte counts and % reticulocytes, while RBC count, hematocrit, and hemoglobin level were not significantly altered (Supporting Information Table S2). A significant (p < 0.05–0.01) elevation of white blood cell (WBC) count in nearly all chelator treatment groups was observed, except for the lower DpC·HCl (4 mg/kg) dose. A significant (p < 0.05–0.01) increase in platelet count was also evident in the 3 and 4 mg/kg doses of Dp4e4mT·HCl and DpC·HCl, respectively.

Histology. Histological examination of the spleen, kidney, liver, heart, lungs, and brain was performed by an independent veterinary pathologist (Rothwell Consulting, Sydney, NSW) after staining tissues with hematoxylin and eosin (H & E; to assess general ultrastructural pathology), Perls' (to detect the presence of Fe-loading), and Gomori Trichrome (for detection of fibrosis) by standard methods.[10,11] Previous tumor xenograft studies with the chelators, 3-AP and Dp44mT, showed that 3-AP increased the number of hematopoietic cells in the splenic red pulp, whereas Dp44mT induced cardiac fibrosis (as demonstrated by Gomori Trichrome staining of cardiac sections) at high nonoptimal doses.[10] In the current study, no increase in hematopoietic cells in the splenic red pulp was found as a result of 21 days of treatment under all conditions (data not shown). Assessment of Perl's stained spleen sections showed no alteration in hemosiderin derived from splenic macrophages that are generally present in the splenic red pulp of normal mice.[11,47] The lack of these changes was consistent with the observation that RBC numbers did not markedly decrease in any treatment group with the exception of only a modest decrease in RBC count in mice treated with the higher DpC·HCl dose (8 mg/kg; Supporting Information Table S2).

In agreement with several studies from our laboratory,[10,11] Dp44mT (0.75 mg/kg) induced fibrotic legions that were particularly evident in the wall of the right ventricle and also in the myocardium beneath the endocardium of the left ventricle (Figure 8D). In contrast, treatment of mice with iv Dp4e4mT·HCl (3 or 6 mg/kg) or DpC·HCl (4 or 8 mg/kg) did not result in any evidence of cardiac fibrosis despite the much higher doses used (Figure 8D).

A previous investigation from our laboratory showed that the structurally related ligand, Bp44mT, caused partially reversible cytoplasmic vacuolation of the liver, particularly when given orally.[11] In the current study, mild vacuolation was evident in the livers of mice treated with Dp44mT and at the higher doses of Dp4e4mT·HCl (6 mg/kg) and DpC·HCl (8 mg/kg). However, there was no evidence of hepatocellular necrosis or fibrosis. The mild cytoplasmic vacuolation of the liver in these groups correlated to a small, but significant (p < 0.05–0.01) increase in liver weights in these groups (Supporting Information Table S1). All other H & E stained organs appeared normal (data not shown), which agreed with the lack

dx.doi.org/10.1021/jm300768u | J. Med. Chem. 2012, 55, 7230–7244

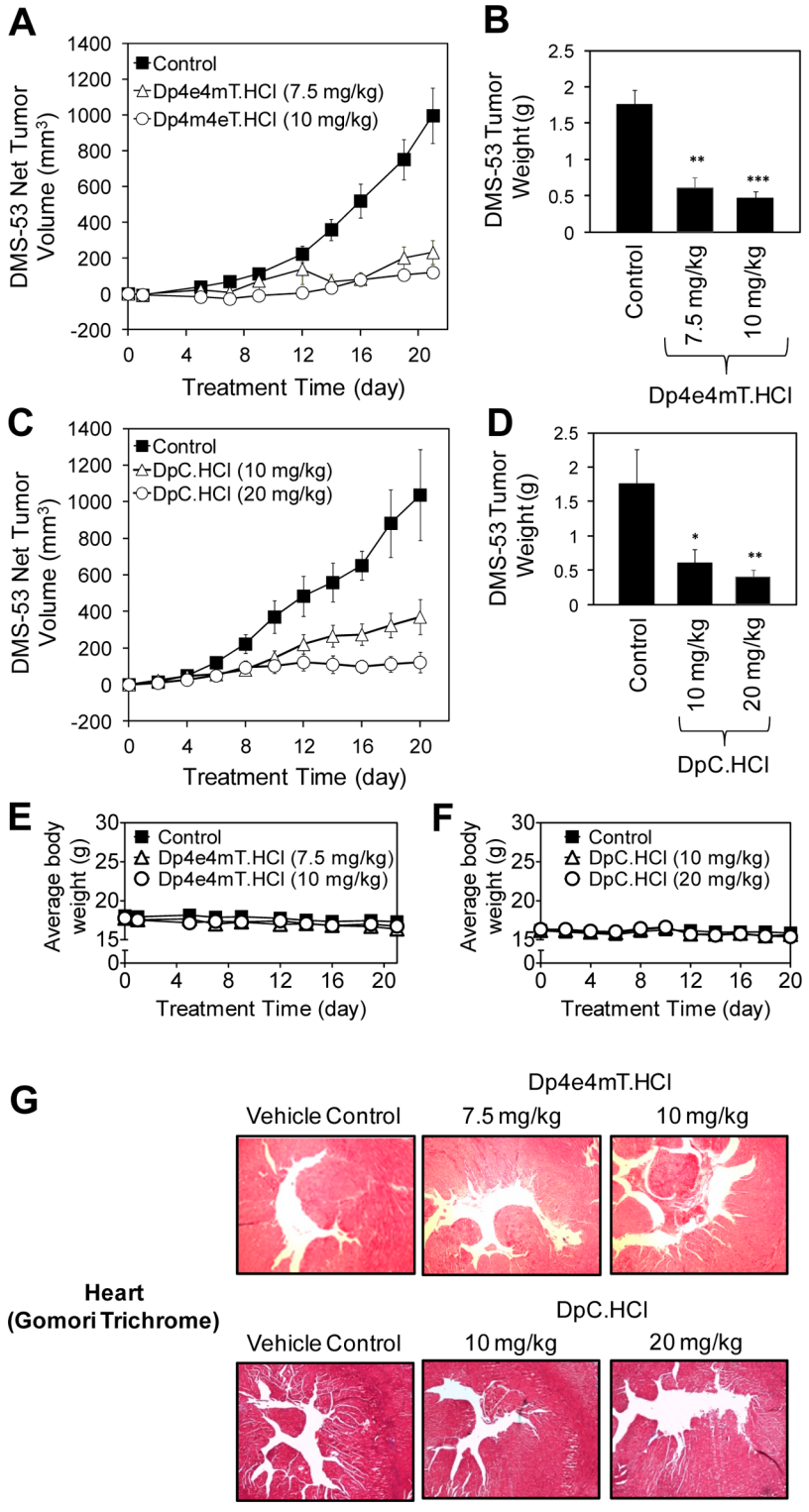

Figure 9. DpC and Dp4e4mT demonstrate marked antitumor activity against primary human DMS-53 lung tumor xenografts in nude mice after oral administration and do not induce cardiotoxicity. (A) Net tumor volume as a function of time of DMS-53 xenografts after oral administration (gavage) of vehicle control (30% propylene glycol/saline) or Dp4e4mT·HCl (7.5 or 10 mg/kg). (B) Tumor weights (wet weight) from the study in (A) after sacrifice of the animals on day 20. (C) Net tumor volume as a function of time of DMS-53 xenografts after oral administration (gavage) of vehicle control (30% propylene glycol/saline) or DpC·HCl (10 or 20 mg/kg). (D) Tumor weights (wet weight) from the study in (C) after sacrifice of the animals on day 20. (E) Average body weights of nude mice for the study in (A) during treatment with the agents for 20 days. (F) Average body weights of nude mice for the study in (C) during treatment with the agents for 20 days. (G) Histological sections of the hearts taken from the mice in (A,C) after 20 days of treatment and stained with Gomori Trichrome to detect fibrosis (magnification 100×). It should be noted that Dp44mT could not be given by the oral route as a relative comparison due to acute toxicity.[11] Results in (A–F) are mean ± SD (n = 6–11 mice/condition), while the photographs in (G) show typical heart histology from the treatment groups.

dx.doi.org/10.1021/jm300768u | J. Med. Chem. 2012, 55, 7230–7244

of change in the weights of these organs in the control and chelator-treated groups (Supporting Information Table S1).

Novel Second-Generation Chelators are also Orally Active against DMS-53 Lung Carcinoma Xenografts. To further assess the potential clinical utility of the second-generation analogues, we also examined whether they exhibited activity after oral administration. Assessment of "Lipinski's Rule of Five" indicated that the DpT class of thiosemicarbazones should be orally available.[48] Initial dose-range finding MTD experiments conducted in DMS-53 tumor-bearing mice suggested good oral activity and showed that the MTDs of Dp4e4mT·HCl and DpC·HCl were 10 and 20 mg/kg, respectively, over a 28-day treatment period (data not shown). Hence, these doses were chosen for examination in more comprehensive tumor growth studies. Because of the rapid toxicity of Dp44mT after oral administration,[11] it was not possible to include it as a positive control. In these studies, mice were gavaged with the vehicle control, Dp4e4mT·HCl, or DpC·HCl 3 times/week using an established protocol in our laboratory for thiosemicarbazones.[11]

After 20 days of treatment, mice bearing DMS-53 tumors receiving the vehicle control grew quickly, reaching an average net volume of 997 ± 155 mm^3, which was close to the maximum ethical limit (1000 mm^3) prescribed by the local ethics committee, and thus, the experiment was terminated at this time (Figure 9A). Doses of Dp4e4mT·HCl at 7.5 and 10 mg/kg markedly and significantly ($p < 0.01–0.001$) reduced the net growth of DMS-53 tumor xenografts to 231 ± 66 mm^3 and 119 ± 20 mm^3, respectively (Figure 9A). Importantly, as observed in the iv studies, measurement of tumor volumes in mice that were treated orally with Dp4e4mT·HCl agreed with excised tumor weights (Figure 9B). Additionally, DpC·HCl when given orally at 10 or 20 mg/kg over 20 days, also significantly ($p < 0.05–0.01$) inhibited tumor growth relative to mice receiving the vehicle control (Figure 9C), and again, these tumor volumes reflected the excised tumor weights (Figure 9D). Notably, because of the significant inhibition of tumor growth observed after oral administration of Dp4e4mT·HCl and DpC·HCl, our results suggest that these chelators may be more effective than the orally administered chemotherapeutic and ribonucleotide reductase inhibitor, hydroxyurea, that shows poor efficacy.[48]

Toxicology Following Oral Administration. Body and Organ Weights. In agreement with the iv administration study, body weights of chelator-treated animals did not significantly change relative to the vehicle control (Figure 9E,F). Furthermore, in most cases, organ weights did not significantly alter between the treated groups and the vehicle control (Supporting Information Table S3 and S4), with the exception that lung and heart weights were slightly, but significantly ($p < 0.05$) higher in the 10 mg/kg Dp4e4mT·HCl-treated group, and the spleen weight was significantly ($p < 0.05$) lower in the 7.5 mg/kg Dp4e4mT·HCl-treated group (Supporting Information Table S3). However, these alterations in weight could not be correlated to histology which was normal (data not shown). These data further indicate that treatment with these two analogues was well tolerated after oral administration.

Hematological Indices. Hematological indices were also examined after oral administration of the two ligands (Supporting Information Tables S5 and S6). In the 7.5 mg/kg Dp4e4mT·HCl-treated group, the hemoglobin level was slightly, but significantly ($p < 0.05$) reduced, while in the 10 mg/kg Dp4e4mT·HCl-treated group, RBC count ($p < 0.05$) and hemoglobin level ($p < 0.01$) were significantly decreased (Supporting Information Table S5). For both the 7.5 and 10 mg/kg Dp4e4mT·HCl-treated groups, the hematocrit was also significantly ($p < 0.05$) reduced. However, in contrast, no significant differences were found in any hematological parameters in the DpC·HCl-treated mice (Supporting Information Table S6), demonstrating the high tolerability of this ligand.

Histology. There were no detectable changes in the spleen, kidney, liver, heart, lungs, or brain after treatment with the two analogues relative to the vehicle control. Importantly, in agreement with the iv studies, oral treatment of mice with Dp4e4mT·HCl or DpC·HCl at any of the doses tested did not induce cardiac fibrosis (Figure 9G).

■ CONCLUSIONS

New drug therapies that are able to overcome existing problems of drug resistance and poor efficacy are urgently required for lung and other solid tumors. We have been actively exploring the activity of a range of Fe chelators as potential cancer treatments. Over the past decade, our research has provided chelator structure–activity relationships that have culminated in the design of the second-generation DpT and BpT analogues presented herein. These new analogues are the most potent antitumor agents our laboratories have designed and overcome the limitations of earlier first-generation chelators, in particular the cardiotoxicity evident with Dp44mT at high, nonoptimal doses.[10]

The specific structural design insight incorporated into the second-generation analogues was "saturation" at the terminal N4 atom with alkyl or aryl groups. This increased the lipophilicity of the second-generation analogues and resulted in superior antiproliferative activity relative to first-generation chelators bearing one alkyl group and a hydrogen atom at the N4 atom (Figure 5A). The best performing chelators, DpC·HCl and Dp4e4mT·HCl, showed pronounced activity against lung tumor xenografts without marked toxicological effects by both the intravenous and oral routes. In particular, the high efficacy and low toxicity of orally administered DpC is of significant note. Clearly, oral administration demonstrates a marked advantage for treating patients relative to the more cumbersome intravenous route. It was also demonstrated that these chelators acted synergistically with standard chemotherapeutics for lung cancer. These results provide a strong basis for rapid preclinical development of Dp4e4mT·HCl and especially DpC·HCl as potential antitumor agents.

■ EXPERIMENTAL PROCEDURES

All commercial reagents were used without further purification. DFO was obtained from Novartis (Basel, Switzerland). The chemotherapeutic agents, cisplatin, etoposide, and gemcitabine, were obtained from Sigma-Aldrich (St. Louis, MO). Dp44mT and the first-generation chelators, Dp4mT, Dp4eT, Dp4pT, Bp4mT, and Bp4eT, were synthesized as described.[9,19] Desferrioxamine (DFO) was from Novartis (Basel, Switzerland).

Second-Generation DpT and BpT Chelators: General Synthesis. The second-generation DpT and BpT chelators were synthesized using a combination of established methods.[19,26] Briefly, carbon disulfide (0.2 mol) was added dropwise to the appropriate amine (0.2 mol; e.g., *N*-methylcyclohexylamine for DpC) in NaOH solution (250 mL, 0.8 M). This mixture was allowed to react until the organic layer disappeared, and this occurred after approximately 4 h. Next, sodium chloroacetate (0.2 mol) was added to the aqueous

extract and allowed to react overnight at room temperature. The addition of concentrated HCl (25 mL) gave the solid carboxymethyl thiocarbamate intermediate. Approximately 0.08 mol of carboxymethyl thiocarbamate was dissolved in 20 mL of hydrazine hydrate plus 10 mL of water. This was followed by five cycles of gentle heating (until fuming) and cooling. The solution was then allowed to stand until fine white crystals of thiosemicarbazide intermediate formed. A solution of this intermediate (10 mmol) in water (15 mL) was added to di-2-pyridyl ketone (10 mmol) dissolved in EtOH (15 mL). Then, 5 drops of glacial acetic acid were added and the mixture was refluxed for 2 h and cooled to 5 °C to give the thiosemicarbazone precipitate. Preparation of the HCl salt for assessment of in vivo antitumor activity was performed by dissolving the ligand (10 mM) in a minimum volume of warm toluene (~60 °C). When the solution had cooled to approximately 40 °C, equimolar HCl was then added to give the HCl salt.

Dp4e4mT and Dp4e4mT·HCl·5H$_2$O. Yield: 44% (from CS_2). Anal. Calcd for $C_{15}H_{17}N_5S·H_2O$: C, 56.76%; H, 6.03%; N, 22.06%. Found: C, 56.61%; H, 6.12%; N, 21.84%. Dp4e4mT·HCl·5H$_2$O: Yield: 91% (from Dp4e4mT). Anal. Calcd for $C_{15}H_{17}N_5S·HCl·5H_2O$: C, 41.42; H, 6.72; N, 16.10%. Found: C, 41.31; H, 6.45; N, 15.95%. ^{1}H NMR (DMSO-d_6): δ 8.84 (d, 1H), 8.66 (d, 1H), 8.13−8.09 (t, 1H), 8.04−7.97 (dt, 2H), 7.67−7.59 (dt, 3H), 3.32 (s, 3H), 1.20 (s, 3H). MS m/z (%) 322.0 (M + Na, 46), 620.87 (M; dimer, + Na, 100).

Dp44eT. Yield: 38% (from CS_2). Anal. Calcd for $C_{16}H_{21}N_5OS·H_2O$: C, 57.98%; H, 6.56%; N, 21.13%. Found: C, 57.87%; H, 6.52%; N, 20.89%. ^{1}H NMR (DMSO-d_6): 8.60 (d, 1H), 8.80 (d, 1H), 7.92 (d, 1H), 7.62 (m, 1H), 7.59 (dd, 1H), 7.43 (t, 1H), 1.25 (t, 6H), 1.14 (q, 4H). MS m/z (%) 314.0 (M + H, 100), 336.1 (M + Na, 24), 648.9 (M; dimer, + Na, 14).

DpC and DpC·HCl·5H$_2$O. Yield: 64% (from CS_2). Anal. Calcd for $C_{19}H_{23}N_5S$: C, 64.56%; H, 6.56%; N, 19.81%. Found: C, 64.51%; H, 6.47%; N, 20.04%. DpC·HCl·5H$_2$O: Yield 87% (from Dp4cycH4mT). Anal. Calcd for $C_{19}H_{23}N_5S·HCl·5H_2O$: C, 47.54%; H, 7.14%; N, 14.59%. Found: C, 47.06%; H, 6.65%; N, 14.95%. ^{1}H NMR (DMSO-d_6): 8.82 (d, 1H), 8.61 (d, 1H), 8.04−7.90 (m, 3H), 7.62−7.56 (t, 2H), 7.50−7.46 (t, 1H), 3.18 (s, 3H), 1.83−1.49 (m, 7H), 1.40−1.10 (m, 3H). MS m/z (%) 376.1 (M + Na, 22), 729.0 (M; dimer + Na, 100).

Dp4p4mT. Yield: 51% (from CS_2). Anal. Calcd for $C_{19}H_{17}N_5$: C, 65.68%; H, 4.93%; N, 20.15%. Found: C, 65.59%; H, 5.16%; N, 20.17%. ^{1}H NMR (DMSO-d_6): 8.55 (s, 1H), 7.95 (t, 1H), 7.84 (q, 1H), 7.75 (d, 1H), 7.65−7.58 (m, 3H), 7.46−7.43 (m, 5H), 7.36 (t, 1H), 2.09 (s, 3H). MS m/z (%) 370.0 (M + Na, 16), 716.8 (M; dimer + Na, 100).

Dp4e4pT. Yield: 57% (from CS_2). Anal. Calcd for $C_{20}H_{19}N_5$: C, 66.45%; H, 5.29%; N, 19.37%. Found: C, 66.06%; H, 5.31%; N, 19.46%. ^{1}H NMR (DMSO-d_6): 8.85 (dt, 1H), 7.94 (t, 1H), 7.82−7.87 (m, 2H), 7.73 (d, 1H), 7.34 (dd, 1H), 7.39 (d, 2H), 7.44 (m, 2H), 7.67−7.59 (m, 3H), 4.25 (q, 2H), 1.17 (t, 3H). MS m/z (%) 384.0 (M + Na, 38), 744.8 (M; dimer + Na, 100).

Bp4m4eT. Yield: 77% (from 4-methyl-4ethyl-3-thiosemicarbazide). Anal. Calcd for $C_{16}H_{18}N_4S$: C, 64.40%; H, 6.07%; N, 18.78%. Found: C, 64.47%; H, 6.18%; N, 18.65%. ^{1}H NMR (DMSO-d_6): 8.87 (d, 1H), 8.02 (dt, 1H), 7.63−7.57 (dd, 1H), 7.56−7.47 (m, 5H), 7.34 (d, 1H), 3.78 (q, 2H), 1.25 (t, 3H). MS m/z (%) 320.8 (M + Na, 27), 618.8 (M; dimer + Na, 100).

Bp44eT. Yield: 68% (from 4,4-diethyl-3-thiosemicarbazide). Anal. Calcd for $C_{17}H_{20}N_4S$: C, 65.35%; H, 6.45%; N, 17.93%. Found: C, 65.32%; H, 6.68%; N, 17.94%. ^{1}H NMR (DMSO-d_6): 8.84 (d, 1H), 8.02 (dt, 1H), 7.62−7.58 (dd, 1H), 7.58−7.47 (m, 5H), 7.34 (d, 1H), 3.86 (q, 4H), 1.28 (t, 6H). MS m/z (%) 313.1 (M + H, 92), 335.1 (M + Na, 100), 646.9 (M; dimer + Na, 19).

Copper Complexes of Selected Second-Generation DpT Chelators. Copper complexes of DpC and Dp4e4mT were synthesized in accordance with established procedures,[27] as described briefly here for [Cu(Dp4e4mT)(OAc)]. Dp4e4mT·H$_2$O (0.317 g, 1 mmol) was dissolved in DMF (7 mL) with gentle heating and stirring. A solution of Cu(OAc)$_2$·3H$_2$O (0.20 g, 1 mmol) in water (7 mL) was added dropwise with stirring, and the ligand solution immediately turned dark brown. A fine olive-green−brown powder formed on standing, which was filtered off, washed with EtOH (5 mL) and then diethyl ether (5 mL), and dried in a vacuum desiccator overnight (yield 41%). Anal. Calcd for $C_{17}H_{19}N_5CuSO_2·H_2O$: C, 46.51%; H, 4.82%; N, 15.95%. Found: C, 46.35%; H 4.73%; N 16.20%. Electronic spectra: (DMF) 302 nm (ε 17700 M^{-1} cm^{-1}), 361 (9100), 434 (18200), (DMF:H$_2$O 2:1) 302 nm (ε 18700 M^{-1} cm^{-1}), 427 (21000). IR (main peaks) 1488s, 1501s, 1433 m, 1370 m, 1311s, 1238 m, 1084 m, 970 m, 880 m, 824 m, 788s, 744 m. MS m/z (%) 361.3 (M − OAc, 100).

Cu(Dp4e4mT)Cl. Yield: 58%. Anal. Calcd for $C_{15}H_{16}N_5CuSCl$: C, 45.34%; H, 4.06%; N, 17.62%. Found: C, 45.25%; H 4.01%; N 17.83%. Electronic spectra: (DMF) 308 nm (ε 15200 M^{-1} cm^{-1}), 364 (8400), 437 (15700), (DMF:H$_2$O 2:1) 303 nm (ε 18000 M^{-1} cm^{-1}), 427 (20000). IR (main peaks) 2973 m, 1593s, 1502s, 1464s, 1398s, 1371 m, 1289 m, 1237 m, 1079w, 1060 m, 984s, 822 m, 782vs, 741 m, 661 m, 634 m. MS m/z (%) 361.3 (M − Cl, 59).

Cu(DpC)(OAc). Yield: 51%. Anal. Calcd for $C_{21}H_{24}N_5CuSO_2$: C, 53.21%; H, 5.01%; N, 14.77%. Found: C, 52.87%; H, 5.24%; N, 14.89%. Electronic spectra: (DMF) 306 nm (ε 17700 M^{-1} cm^{-1}), 370 (9700), 437 (19500), (DMF:H$_2$O 2:1) 304 nm (ε 16600 M^{-1} cm^{-1}), 430 (19500). IR (main peaks) 2923 m, 1615 m, 1593 m, 1448 m, 1375vs, 1304vs, 1247s, 1182 m, 1152 m, 1085 m, 1003s, 926 m, 883 m,827w, 782s, 739s, 649 m. MS m/z (%) 415.4 (M − OAc, 100).

Cu(DpC)Cl. Yield: 43%. Anal. Calcd for $C_{19}H_{22}N_5CuSCl$: C, 50.55%; H, 4.91%; N, 15.51%. Found: C, 50.38%; H 4.85%; N 15.75%. Electronic spectra: (DMF) 310 nm (ε 17200 M^{-1} cm^{-1}), 371 (9900), 440 (18800), (DMF:H$_2$O 2:1) 305 nm (ε 16200 M^{-1} cm^{-1}), 430 (19900). IR (main peaks) 2924 m, 1592s, 1448vs, 1398s, 1370s, 1247s, 1301vs, 1244vs, 1179 m, 1154s, 1083 m, 1002vs, 883 m, 785s, 739 m, 655 m. MS m/z (%) 415.4 (M − Cl, 100).

Physical Methods. ^{1}H NMR (400 MHz) spectra were acquired using a Bruker Avance 400 NMR spectrometer with DMSO-d_6 as the solvent and internal reference (Me_2SO: ^{1}H NMR δ 2.49 ppm and ^{13}C NMR δ 39.5 ppm vs TMS). Infrared spectra were measured with a Varian Scimitar 800 FT-IR spectrophotometer with compounds being dispersed as KBr discs or a Perkin-Elmer 1600 series spectrometer using an ATR sample holder. Electronic spectra were measured with a Perkin-Elmer Lambda 35 spectrophotometer. Cyclic voltammetry was determined with a BAS 100B/W potentiostat utilizing a glassy carbon working electrode and a Pt counter electrode. For experiments done in DMF:water (7:3), a Ag/AgCl reference electrode was used. Potentials are given relative to the NHE. For experiments in 100% DMF, a nonaqueous Ag/Ag$^+$ (DMF) electrode was constructed and the potentials were referenced externally against the ferrocene/ferrocenium couple. All solutions contained 0.1 M Et_4NClO_4 as supporting electrolyte and were purged with Ar before measurement. Electron paramagnetic resonance (EPR) spectra were measured on a Bruker ER200 instrument at X-band frequency (~9.3 GHz) in 1 mM DMSO frozen solutions at 77 K. Spectra were simulated with the program EPR50F.[49] Log P_{calc} values were the average log P values calculated in ChemDraw v4.5 using Crippen's fragmentation,[50] Viswanadhan's fragmentation,[51] and Broto's methods.[52]

X-ray Crystallography. Crystallographic data were acquired at 293 K on an Oxford Diffraction Gemini CCD diffractometer employing graphite-monochromated Cu Kα radiation (1.5418 Å) and operating within the range $2 < 2\theta < 125°$. Data reduction and empirical absorption corrections (multiscan) were performed with the Oxford Diffraction CrysAlisPro software. The structure was solved by direct methods with SHELXS and refined by full-matrix least-squares analysis with SHELXL-97.[53] All non-H atoms were refined with anisotropic thermal parameters. Molecular structure diagrams were produced with ORTEP3,[54] and all calculations were carried out within the WinGX package.[55] The data in CIF format has been deposited at the Cambridge Crystallographic Data Centre with deposition number CCDC 883394.

Cell Culture. Human SK-N-MC neuroepithelioma cells, human MRC5 fibroblasts, human DMS-53 small cell lung carcinoma cells, and human A549 nonsmall cell lung carcinoma cells were obtained from the American Type Culture Collection (Manassas, VA) and grown as

described.[10,11] Cells were used within 2 months of purchase after resuscitation of frozen aliquots. Cell lines were authenticated based on viability, recovery, growth, morphology, and also cytogenetic analysis, antigen expression, DNA profile, and iso-enzymology by the provider.

Cellular Proliferation Assay and Synergism Calculations. The effect of chelators on cellular proliferation after a 72 h/37 °C incubation was assessed using MTT assays as previously described.[35] Direct cell counts were used to validate MTT assays.[35] The effect of multiple drug combinations on the proliferation of DMS-53 and A549 cells was also examined using the MTT assay. Combinations of gemcitabine and cisplatin with Dp4e4mT·HCl and DpC·HCl, as well as the control chelators, DFO and Dp44mT, were assessed. The dose−response curves were analyzed using the methodology of Chou and Talalay.[45] Briefly, the median-effect plot and multiple-drug equation derived by Chou and Talalay[45] was employed to determine the CI using CalcuSyn (Biosoft, Cambridge, MA).

Preparation of ^{56}Fe- and ^{59}Fe-Tf. Human Tf (Sigma-Aldrich) was labeled with ^{56}Fe or ^{59}Fe (Dupont NEN, MA) to produce ^{59}Fe-Tf and ^{56}Fe-Tf, respectively, as previously described.[35,56,57] Briefly, unbound ^{56}Fe or ^{59}Fe was removed by passage through a Sephadex G25 column and exhaustive vacuum dialysis against a large excess of 0.15 M NaCl buffered to pH 7.4 with 1.4% $NaHCO_3$ by standard methods.[56,57]

Effect of Chelators on ^{59}Fe Efflux from Cells. Iron efflux experiments examining the ability of various chelators to mobilize ^{59}Fe from SK-N-MC cells were performed using established techniques.[35] Briefly, following prelabeling of cells with ^{59}Fe-Tf (0.75 μM) for 3 h/37 °C, the cell cultures were washed on ice four times with ice-cold PBS and then subsequently incubated with each chelator (25 μM) for 3 h/37 °C. The overlying media containing released ^{59}Fe was then separated from the cells using a Pasteur pipet. The radioactivity was measured in both the cell pellet and the supernatant using a γ-scintillation counter (Wallac Wizard 3, Turku, Finland). In these studies, the novel ligands were compared to the previously characterized chelators, DFO, NIH, and Dp44mT.[12,35]

Effect of Chelators at Preventing ^{59}Fe Uptake from ^{59}Fe-Tf by Cells. The ability of the chelators to prevent cellular ^{59}Fe uptake from the serum Fe transport protein, ^{59}Fe-Tf, was examined using established techniques.[35] Briefly, cells were incubated with ^{59}Fe-Tf (0.75 μM) for 3 h/37 °C in the presence of each of the chelators (25 μM). The cells were then washed four times with ice-cold PBS, and internalized ^{59}Fe was determined by standard techniques by incubating the cell monolayer for 30 min/4 °C with the general protease, Pronase (1 mg/mL; Sigma-Aldrich). The cells were removed from the monolayer using a plastic spatula and centrifuged at 14000 rpm/1 min. The supernatant represents membrane-bound, Pronase-sensitive ^{59}Fe that was released by the protease, while the Pronase-insensitive fraction represents internalized ^{59}Fe.[35] The novel ligands were compared to the previously characterized chelators, DFO, NIH, and Dp44mT.[12,35]

Tumor Xenograft Model in Nude Mice. All procedures for the animal experiments were approved by the University of Sydney Animal Ethics Committee. Female BALB/c nu/nu mice were used at 8−10 weeks of age (Laboratory Animal Services, University of Sydney). Mice were housed under a 12 h light−dark cycle, routinely fed basal rodent chow, and watered ad libitum. DMS-53 human tumor cells were harvested and resuspended in a solution containing 1:1 ratio of RPMI and Matrigel (BD Biosciences, San Jose, CA). Viable cells (5×10^6 cells), as determined using trypan blue dye exclusion, were subcutaneously injected into the right flanks of mice. Tumor size was measured using digital Vernier calipers after engraftment and volume was calculated, as described.[58,59] The chelator treatment began after the tumors reached a volume of 100 mm^3.

In Vivo Chelator Administration. Chelators were dissolved in 30% propylene glycol in 0.9% saline. During the intravenous (iv) studies, chelators were injected (100 μL) into the tail vein of nude mice using a 19 gauge needle, 5 days/week (Monday−Friday). In the oral administration experiments, chelators were given via oral gavage (300 μL) on alternate days, 3 times/week, for the indicated time periods (see Results) by standard methods.[11] As a relevant control, mice were either iv injected or gavaged with the vehicle alone (30% propylene glycol/0.9% saline).

Hematology. Blood was collected from the hearts of anesthetized mice by cardiac puncture at the end of the experiment. Serum clinical and hematological parameters were determined using a Konelab 20i analyzer (Thermo-Electron Corporation, Vantaa, Finland) and Sysmex K-4500 analyzer (TOA Medical Electronics Co., Kobe, Japan), respectively.

Histology. Organs were dissected, fixed in 10% formalin, sectioned, and stained with hematoxylin and eosin, Perl's, or Gomori Trichrome stains for microscopic examination, as described.[11]

Statistics. Results are expressed as mean ± standard deviation (SD). Statistical analysis comparing two groups was performed using Student's *t*-test. Data were considered statistically significant when $p < 0.05$.

■ ASSOCIATED CONTENT

Ⓢ Supporting Information

Body and organ weights, hematological indices from in vivo tumor xenograft experiments, experimental and simulated EPR spectra, and cyclic voltammetry of Cu complexes. This material is available free of charge via the Internet at http://pubs.acs.org.

■ AUTHOR INFORMATION

Corresponding Author

*Phone: +61-2-9036-6548. Fax: +61-2-9036-6549. E-mail: d.richardson@med.usyd.edu.au.

Notes

The authors declare no competing financial interest.

■ ACKNOWLEDGMENTS

This work was supported by: a project grant from the National Health and Medical Research Council (NHMRC) Australia to D.R.R. (grant 632778), a NHMRC Senior Principal Research Fellowship to D.R.R. (grant 571123), a Cancer Institute New South Wales Early Career Development Fellowship to D.B.L. (grant 07/ECF/1-19), a Cancer Institute New South Wales Early Career Development Fellowship to P.J.J. (grant 10/ECF/2-15) and D.S.K. (grant 08/ECF/1-30), a Cancer Institute Research Innovation Grant to D.R.R. and D.S.K. (grant 10/RFG/2-50), a Australian Research Council Discovery Grant to P.V.B. (grant DP1096029), and a King Abdul Aziz University Scholarship to M.B. (grant Jeddah, Saudi Arabia).

■ ABBREVIATIONS USED

3-AP, 3-aminopyridine-2-carboxaldehyde thiosemicarbazone; DFO, desferrioxamine; BpT, 2-benzoylpyridine thiosemicarbazone; Bp4mT, 2-benzoylpyridine 4-methyl-3-thiosemicarbazone; Bp4eT, 2-benzoylpyridine 4-ethyl-3-thiosemicarbazone; Bp44mT, 2-benzoylpyridine 4,4-dimethyl-3-thiosemicarbazone; Bp4e4mT, 2-benzoylpyridine 4-ethyl-4-methyl-3-thiosemicarbazone; Bp44eT, 2-benzoylpyridine 4,4-diethyl-3-thiosemicarbazone; CI, combination index; DpT, di-2-pyridyl ketone thiosemicarbazone; Dp44mT, di-2-pyridyl ketone 4,4-dimethyl-3-thiosemicarbazone; DpC, di-2-pyridyl ketone 4-cyclohexyl-4-methyl-3-thiosemicarbazone; Dp4e4mT, di-2-pyridyl ketone 4-ethyl-4-methyl-3-thiosemicarbazone; Dp44eT, di-2-pyridyl ketone 4,4-diethyl-3-thiosemicarbazone; Dp4p4mT, di-2-pyridyl ketone 4-phenyl-4-methyl-3-thiosemicarbazone; Dp4p4eT, di-2-pyridyl ketone 4-phenyl-4-ethyl-3-thiosemicarbazone; MTD, maximum tolerated dose; NIH, 2-hydroxy-1-naphthaldehyde isonicotinoyl hydrazone; ROS, reactive oxygen species; Tf, transferrin

REFERENCES

(1) Kovacevic, Z.; Kalinowski, D. S.; Lovejoy, D. B.; Quach, P.; Wong, J.; Richardson, D. R. Iron Chelators: Development of Novel Compounds with High and Selective Anti-Tumour Activity. *Curr. Drug Delivery* **2010**, *7*, 194−207.

(2) Yu, Y.; Wong, J.; Lovejoy, D. B.; Kalinowski, D. S.; Richardson, D. R. Chelators at the Cancer Coalface: Desferrioxamine to Triapine and Beyond. *Clin. Cancer Res.* **2006**, *12*, 6876−6883.

(3) Nyholm, S.; Mann, G. J.; Johansson, A. G.; Bergeron, R. J.; Graslund, A.; Thelander, L. Role of Ribonucleotide Reductase in Inhibition of Mammalian Cell Growth by Potent Iron Chelators. *J. Biol. Chem.* **1993**, *268*, 26200−26205.

(4) Saletta, F.; Kovacevic, Z.; Richardson, D. R. Iron chelation: Deciphering Novel Molecular Targets for Cancer Therapy. The Tip of the Iceberg of a Web of Iron-Regulated Molecules. *Future Med. Chem.* **2011**, *3*, 1983−1986.

(5) Yu, Y.; Gutierrez, E.; Kovacevic, Z.; Saletta, F.; Obeidy, P.; Rahmanto, Y. S.; Richardson, D. R. Iron Chelators for the Treatment of Cancer. *Curr. Med. Chem.* **2012**, *19*, 2689−2702.

(6) Pahl, P. M.; Horwitz, L. D. Cell Permeable Iron Chelators as Potential Cancer Chemotherapeutic Agents. *Cancer Invest.* **2005**, *23*, 683−691.

(7) Knox, J. J.; Hotte, S. J.; Kollmannsberger, C.; Winquist, E.; Fisher, B.; Eisenhauer, E. A. Phase II Study of Triapine in Patients with Metastatic Renal Cell Carcinoma: A Trial of the National Cancer Institute of Canada Clinical Trials Group (NCIC IND.161). *Invest. New Drugs* **2007**, *25*, 471−477.

(8) Ma, B.; Goh, B. C.; Tan, E. H.; Lam, K. C.; Soo, R.; Leong, S. S.; Wang, L. Z.; Mo, F.; Chan, A. T.; Zee, B.; Mok, T. A Multicenter Phase II Trial of 3-Aminopyridine-2-carboxaldehyde Thiosemicarbazone (3-AP, Triapine) and Gemcitabine in Advanced Non-Small-Cell Lung Cancer with Pharmacokinetic Evaluation using Peripheral Blood Mononuclear Cells. *Invest. New Drugs* **2008**, *26*, 169−173.

(9) Kalinowski, D. S.; Yu, Y.; Sharpe, P. C.; Islam, M.; Liao, Y. T.; Lovejoy, D. B.; Kumar, N.; Bernhardt, P. V.; Richardson, D. R. Design, Synthesis, and Characterization of Novel Iron Chelators: Structure−Activity Relationships of the 2-Benzoylpyridine Thiosemicarbazone Series and their 3-Nitrobenzoyl Analogues as Potent Antitumor Agents. *J. Med. Chem.* **2007**, *50*, 3716−3729.

(10) Whitnall, M.; Howard, J.; Ponka, P.; Richardson, D. R. A Class of Iron Chelators with a Wide Spectrum of Potent Antitumor Activity that Overcomes Resistance to Chemotherapeutics. *Proc. Natl. Acad. Sci. U.S.A.* **2006**, *103*, 14901−14906.

(11) Yu, Y.; Rahmanto, Y. S.; Richardson, D. R. Bp44mT: An Orally Active Iron Chelator of the Thiosemicarbazone Class with Potent Anti-Tumour Efficacy. *Br. J. Pharmacol.* **2012**, *165*, 148−166.

(12) Yuan, J.; Lovejoy, D. B.; Richardson, D. R. Novel Di-2-pyridyl-Derived Iron Chelators with Marked and Selective Antitumor Activity: In Vitro and In Vivo Assessment. *Blood* **2004**, *104*, 1450−1458.

(13) Quach, P.; Gutierrez, E.; Basha, M. T.; Kalinowski, D. S.; Sharpe, P. C.; Lovejoy, D. B.; Bernhardt, P. V.; Jansson, P. J.; Richardson, D. R. Methemoglobin Formation by 3-AP, Dp44mT and Other Anti-Cancer Thiosemicarbazones: Identification of Novel Thiosemicarbazones and Therapeutics that Prevent this Effect. *Mol. Pharmacol.* **2012**, *82*, 105−114.

(14) Kovacevic, Z.; Chikhani, S.; Lovejoy, D. B.; Richardson, D. R. Novel Thiosemicarbazone Iron Chelators Induce Up-Regulation and Phosphorylation of the Metastasis Suppressor N-Myc Down-Stream Regulated Gene 1: A New Strategy for the Treatment of Pancreatic Cancer. *Mol. Pharmacol.* **2011**, *80*, 598−609.

(15) Rao, V. A.; Klein, S. R.; Agama, K. K.; Toyoda, E.; Adachi, N.; Pommier, Y.; Shacter, E. B. The Iron Chelator Dp44mT causes DNA Damage and Selective Inhibition of Topoisomerase IIalpha in Breast Cancer Cells. *Cancer Res.* **2009**, *69*, 948−957.

(16) Tian, J.; Peehl, D. M.; Zheng, W.; Knox, S. J. Antitumor and Radiosensitization Activities of the Iron Chelator HDp44mT are Mediated by Effects on Intracellular Redox Status. *Cancer Lett.* **2010**, *298*, 231−237.

(17) Jansson, P. J.; Hawkins, C. L.; Lovejoy, D. B.; Richardson, D. R. The Iron Complex of Dp44mT is Redox-Active and Induces Hydroxyl Radical Formation: An EPR Study. *J. Inorg. Biochem.* **2010**, *104*, 1224−1228.

(18) Lovejoy, D. B.; Jansson, P. J.; Brunk, U. T.; Wong, J.; Ponka, P.; Richardson, D. R. Antitumor Activity of Metal-Chelating Compound Dp44mT is Mediated by Formation of a Redox-Active Copper Complex that Accumulates in Lysosomes. *Cancer Res.* **2011**, *71*, 5871−5880.

(19) Richardson, D. R.; Sharpe, P. C.; Lovejoy, D. B.; Senaratne, D.; Kalinowski, D. S.; Islam, M.; Bernhardt, P. V. Dipyridyl Thiosemicarbazone Chelators with Potent and Selective Antitumor Activity Form Iron Complexes with Redox Activity. *J. Med. Chem.* **2006**, *49*, 6510−6521.

(20) Kovacevic, Z.; Chikhani, S.; Lui, G. Y.; Sivagurunathan, S.; Richardson, D. R. The Iron-Regulated Metastasis Suppressor NDRG1 Targets NEDD4L, PTEN, and SMAD4 and Inhibits the PI3K and Ras Signaling Pathways. *Antioxid. Redox Signal.* **2012**, [online early access] PMID 22462691, published online May 8, 2012 , DOI 10.1089/ars.2011.4273 .

(21) Le, N. T.; Richardson, D. R. Iron Chelators with High Antiproliferative Activity Up-Regulate the Expression of a Growth Inhibitory and Metastasis Suppressor Gene: A Link Between Iron Metabolism and Proliferation. *Blood* **2004**, *104*, 2967−2975.

(22) Liu, W.; Xing, F.; Iiizumi-Gairani, M.; Okuda, H.; Watabe, M.; Pai, S. K.; Pandey, P. R.; Hirota, S.; Kobayashi, A.; Mo, Y. Y.; Fukuda, K.; Li, Y.; Watabe, K. N-myc Downstream Regulated Gene 1 Modulates Wnt-Beta-Catenin Signalling and Pleiotropically Suppresses Metastasis. *EMBO Mol. Med.* **2012**, *4*, 93−108.

(23) Gao, J.; Richardson, D. R. The Potential of Iron Chelators of the Pyridoxal Isonicotinoyl Hydrazone Class as Effective Antiproliferative Agents, IV: The Mechanisms Involved in Inhibiting Cell-Cycle Progression. *Blood* **2001**, *98*, 842−850.

(24) Saletta, F.; Rahmanto, Y. S.; Siafakas, A. R.; Richardson, D. R. Cellular Iron Depletion and the Mechanisms Involved in the Iron-Dependent-Regulation of the Growth Arrest and DNA Damage Family of Genes. *J. Biol. Chem.* **2011**, *286*, 35396−35406.

(25) Lovejoy, D. B.; Richardson, D. R. Novel "Hybrid" Iron Chelators Derived from Aroylhydrazones and Thiosemicarbazones Demonstrate Selective Antiproliferative Activity Against Tumor Cells. *Blood* **2002**, *100*, 666−676.

(26) Scovill, J. P. A Facile Synthesis of Thiosemicarbazides and Thiosemicarbazones by the Transamination of 4-Methyl-4-phenyl-3-thiosemicarbazide. *Phosphorus, Sulfur Silicon Relat. Elem.* **1991**, *60*, 15−19.

(27) Jansson, P. J.; Sharpe, P. C.; Bernhardt, P. V.; Richardson, D. R. Novel Thiosemicarbazones of the ApT and DpT Series and their Copper Complexes: Identification of Pronounced Redox Activity and Characterization of their Antitumor Activity. *J. Med. Chem.* **2010**, *53*, 5759−5769.

(28) Richardson, D. R.; Kalinowski, D. S.; Richardson, V.; Sharpe, P. C.; Lovejoy, D. B.; Islam, M.; Bernhardt, P. V. 2-Acetylpyridine Thiosemicarbazones are Potent Iron Chelators and Antiproliferative Agents: Redox Activity, Iron Complexation and Characterization of their Antitumor Activity. *J. Med. Chem.* **2009**, *52*, 1459−1470.

(29) Addison, A. W.; Rao, T. N.; Reedijk, J.; Vanrijn, J.; Verschoor, G. C. Synthesis, Structure, and Spectroscopic Properties of Copper(II) Compounds Containing Nitrogen Sulfur Donor Ligands—The Crystal and Molecular Structure of Aqua[1,7-bis(*N*-methylbenzimidazol-2′-yl)-2,6-dithiaheptane]copper(II) perchlorate. *Dalton Trans.* **1984**, 1349−1356.

(30) Ali, M. A.; Mirza, A. H.; Butcher, R. J.; Bernhardt, P. V.; Karim, M. R. Self-Assembling Dicopper(II) Complexes of Di-2-pyridyl Ketone Schiff Base Ligands Derived from *S*-Alkyldithiocarbazates. *Polyhedron* **2011**, *30*, 1478−1486.

(31) Ali, M. A.; Mirza, A. H.; Nazimuddin, M.; Ahmed, R.; Gahan, L. R.; Bernhardt, P. V. Synthesis and Characterization of Mono- and Bis-Ligand Zinc(II) and Cadmium(II) Complexes of the Di-2-pyridylketone Schiff Base of *S*-Benzyl Dithiocarbazate (Hdpksbz)

and the X-ray Crystal Structures of the [Zn(dpksbz)(2)] and [Cd(dpksbz)NCS](2) Complexes. *Polyhedron* **2003**, *22*, 1471−1479.
(32) Hathaway, B. J. A New Look at the Stereochemistry and Electronic-Properties of Complexes of the Copper(II) Ion. *Struct. Bonding (Berlin, Ger.)* **1984**, *57*, 55−118.
(33) Hamid, M. H. S. A.; Ali, M. A.; Mirza, A. H.; Bernhardt, P. V.; Moubaraki, B.; Murray, K. S. Magnetic, Spectroscopic and X-ray Crystallographic Structural Studies on Copper(II) Complexes of Tridentate NNS Schiff Base Ligands formed from 2-Acetylpyrazine and *S*-Methyl- and *S*-Benzyldithiocarbazates. *Inorg. Chim. Acta* **2009**, *362*, 3648−3656.
(34) Kalinowski, D. S.; Sharpe, P. C.; Bernhardt, P. V.; Richardson, D. R. Design, Synthesis, and Characterization of New Iron Chelators with Anti-Proliferative Activity: Structure−Activity Relationships of Novel Thiohydrazone Analogues. *J. Med. Chem.* **2007**, *50*, 6212−6225.
(35) Richardson, D. R.; Tran, E. H.; Ponka, P. The Potential of Iron Chelators of the Pyridoxal Isonicotinoyl Hydrazone Class as Effective Antiproliferative Agents. *Blood* **1995**, *86*, 4295−4306.
(36) Stefani, C.; Punnia-Moorthy, G.; Lovejoy, D. B.; Jansson, P. J.; Kalinowski, D. S.; Sharpe, P. C.; Bernhardt, P. V.; Richardson, D. R. Halogenated 2′-Benzoylpyridine Thiosemicarbazone (XBpT) Chelators with Potent and Selective Antineoplastic Activity: Relationship to Intracellular Redox Activity. *J. Med. Chem.* **2011**, *54*, 6936−6948.
(37) Yu, Y.; Suryo Rahmanto, Y.; Hawkins, C. L.; Richardson, D. R. The Potent and Novel Thiosemicarbazone Chelators Di-2-pyridylketone-4,4-dimethyl-3-thiosemicarbazone and 2-Benzoylpyridine-4,4-dimethyl-3-thiosemicarbazone Affect Crucial Thiol Systems Required for Ribonucleotide Reductase Activity. *Mol. Pharmacol.* **2011**, *79*, 921−931.
(38) Nurtjahja-Tjendraputra, E.; Fu, D.; Phang, J. M.; Richardson, D. R. Iron Chelation Regulates Cyclin D1 Expression via the Proteasome: A Link to Iron Deficiency-Mediated Growth Suppression. *Blood* **2007**, *109*, 4045−4054.
(39) Richardson, D. R.; Lovejoy, D. B. Dipyridyl thiosemicarbazone compounds and use in therapy. Provisional Patent Application number 2010905539, 2010.
(40) D'Addario, G.; Fruh, M.; Reck, M.; Baumann, P.; Klepetko, W.; Felip, E. Metastatic Non-Small-Cell Lung Cancer: ESMO Clinical Practice Guidelines for Diagnosis, Treatment and Follow-Up. *Ann. Oncol.* **2010**, *21* (Suppl 5), v116−v119.
(41) Simon, G. R.; Turrisi, A. Management of Small Cell Lung Cancer: ACCP Evidence-Based Clinical Practice Guidelines (2nd edition). *Chest* **2007**, *132*, 324S−339S.
(42) Sorensen, M.; Pijls-Johannesma, M.; Felip, E. Small-Cell Lung Cancer: ESMO Clinical Practice Guidelines for Diagnosis, Treatment and Follow-Up. *Ann. Oncol.* **2010**, *21* (Suppl 5), v120−v125.
(43) Chou, T. C. Preclinical versus Clinical Drug Combination Studies. *Leuk. Lymphoma* **2008**, *49*, 2059−2080.
(44) Chou, T. C. Drug Combination Studies and their Synergy Quantification using the Chou−Talalay Method. *Cancer Res.* **2010**, *70*, 440−446.
(45) Chou, T. C.; Talalay, P. Quantitative Analysis of Dose−Effect Relationships: The Combined Effects of Multiple Drugs or Enzyme Inhibitors. *Adv. Enzyme Regul.* **1984**, *22*, 27−55.
(46) Chou, T. C. Theoretical Basis, Experimental Design, and Computerized Simulation of Synergism and Antagonism in Drug Combination Studies. *Pharmacol. Rev.* **2006**, *58*, 621−681.
(47) Suttie, A. W. Histopathology of the Spleen. *Toxicol. Pathol.* **2006**, *34*, 466−503.
(48) Yu, Y.; Kalinowski, D. S.; Kovacevic, Z.; Siafakas, A. R.; Jansson, P. J.; Stefani, C.; Lovejoy, D. B.; Sharpe, P. C.; Bernhardt, P. V.; Richardson, D. R. Thiosemicarbazones from the Old to New: Iron Chelators that are More than just Ribonucleotide Reductase Inhibitors. *J. Med. Chem.* **2009**, *52*, 5271−5294.
(49) Martinelli, R. A.; Hanson, G. R.; Thompson, J. S.; Holmquist, B.; Pilbrow, J. R.; Auld, D. S.; Vallee, B. L. Characterization of the Inhibitor Complexes of Cobalt Carboxypeptidase A by Electron Paramagnetic Resonance Spectroscopy. *Biochemistry* **1989**, *28*, 2251−2258.
(50) Ghose, A. K.; Crippen, G. M. Atomic Physicochemical Parameters for Three-Dimensional-Structure-Directed Quantitative Structure−Activity Relationships. 2. Modeling Dispersive and Hydrophobic Interactions. *J. Chem. Inf. Comput. Sci.* **1987**, *27*, 21−35.
(51) Viswanadhan, V. N.; Ghose, A. K.; Revankar, G. R.; Robins, R. K. Atomic Physiochemical Parameters for 3-Dimensional-Structure Directed Quantitative Structure−Activity Relationships 4. Additional Parameters for Hydrophobic and Dispersive Interactions and their Application for an Automated Superposition of Certain Naturally-Occuring Nucleoside Antibiotics. *J. Chem. Inf. Comput. Sci.* **1987**, *29*, 163−172.
(52) Broto, P.; Moreau, G.; Vandycke, C. Molecular Structures: Perception, Autocorrelation Descriptor and SAR Studies. System of Atomic Contributions for the Calculation of the *n*-Octanol/Water Partition Coefficients. *Eur. J. Med. Chem. Chim. Theor.* **1984**, *19*, 71−78.
(53) Sheldrick, G. A Short History of SHELX. *Acta Crystallogr., Sect. A: Found. Crystallogr.* **2008**, *64*, 112−122.
(54) Farrugia, L. J. ORTEP-3 for Windows—A Version of ORTEP-III with a Graphical User Interface (GUI). *J. Appl. Crystallogr.* **1997**, *30*, 565.
(55) Farrugia, L. J. WINGX—An Integrated System of Windows Programs for the Solution, Refinement and Analysis of Single Crystal X-Ray Diffraction Data. *J. Appl. Crystallogr.* **1999**, *32*, 837−838.
(56) Richardson, D. R.; Baker, E. The Uptake of Iron and Transferrin by the Human Malignant Melanoma Cell. *Biochim. Biophys. Acta* **1990**, *1053*, 1−12.
(57) Richardson, D. R.; Baker, E. Two Mechanisms of Iron Uptake from Transferrin by Melanoma Cells. The Effect of Desferrioxamine and Ferric Ammonium Citrate. *J. Biol. Chem.* **1992**, *267*, 13972−13979.
(58) Balsari, A.; Tortoreto, M.; Besusso, D.; Petrangolini, G.; Sfondrini, L.; Maggi, R.; Menard, S.; Pratesi, G. Combination of a CpG-Oligodeoxynucleotide and a Topoisomerase I Inhibitor in the Therapy of Human Tumour Xenografts. *Eur. J. Cancer* **2004**, *40*, 1275−1281.
(59) Sanceau, J.; Poupon, M. F.; Delattre, O.; Sastre-Garau, X.; Wietzerbin, J. Strong Inhibition of Ewing Tumor Xenograft Growth by Combination of Human Interferon-alpha or Interferon-beta with Ifosfamide. *Oncogene* **2002**, *21*, 7700−7709.